On Maximizing Argon Engines' Performance via Subzero Intake Temperatures in HCCI Mode at High Compression Ratios

Thesis by

Ali Elkhazraji

In Partial Fulfillment of the Requirements

For the Degree of

Master of Science in Mechanical Engineering

King Abdullah University of Science and Technology

Thuwal, Kingdom of Saudi Arabia

March 2020

EXAMINATION COMMITTEE PAGE

The thesis of Ali Elkhazraji is approved by the examination committee.

Committee Chairperson: Prof. Bengt Johansson
Committee Members: Prof. Gaetano Magnotti, Prof. Boon S. Ooi

ABSTRACT

On Maximizing Argon Engines' Performance via Subzero Intake Temperatures in HCCI Mode at High Compression Ratios

Ali Elkhazraji

The improvement of the indicated thermal efficiency of an argon power cycle (replacing nitrogen with argon in the combustion reaction) is investigated in a CFR engine at high compression ratios in homogeneous charge compression ignition (HCCI) mode. The study combines the two effects that can increase the thermodynamic efficiency as predicted by the ideal Otto cycle: high specific heat ratio (provided by argon), and high compression ratios. However, since argon has relatively low heat capacity (at constant volume), it results in high in-cylinder temperatures, which in turn, leads to the occurrence of knock. Knock limits the feasible range of compression ratios and further increasing the compression ratio can cause serious damage to the engine due to the high pressure rise rate caused by advancing the combustion phasing. The technique proposed in this study in order to avoid intense knock of an argon cycle at high compression ratios is to cool the intake charge to subzero temperatures which leads to lower in-cylinder temperatures and hence, less possibility of having knock. The main variable in this study was the intake temperature which was investigated at 40.0 °C and -6.0 °C which corresponded to low and high compression ratios, respectively. Emission analysis shows that the low in-cylinder temperature of the cooled case led to less complete combustion, and so, lower combustion efficiency. Since nitrogen is replaced with argon, NO_x was only formed in negligible amounts due to some nitrogen traces in

the used gasses cylinders. Furthermore, the cooled charge required more work to be done in the gas exchange process due to the decrease in the intake pressure caused by cooling the intake which deteriorated the gas exchange efficiency. The heat losses factor was found to be the main parameter that dictated the improvement of the thermodynamic efficiency and it was found that the indicated thermal efficiency was deteriorated for the cooled case as a result of all the aforementioned factors. Although the values of the thermodynamic efficiency at high compression ratios did not meet the expectations based on the ideal Otto cycle due to the assumptions of the ideal cycle, the obtained values, in general, are relatively high.

ACKNOWLEDGEMENTS

In the name of Allah, the Most Gracious, the Most Merciful. All praise and thanks be to Allah for blessing me with everything I needed to reach where I am. I would like to thank my parents who always believed in me along the journey. They pushed me all the way from teaching me how to write until writing an acknowledgement for them in my Master's thesis. I will forever appreciate them giving me all the support I needed and more.

I would also like to thank my advisor, Prof. Bengt Johansson. A student cannot possibly ask for a better advisor. I am grateful to him for continuously providing me and my colleagues with all the support and guidance that we need and for being very understanding when things do not work out as planned. Furthermore, saying that I am one of his students to anyone in combustion research makes me feel so proud and inspires me to achieve more and to that I am grateful.

I extend my thanks to the committee members, Prof. Gaetano Magnotti and Prof. Boon S. Ooi who agreed to spend time and effort to be in my committee. I also would like to thank the co-authors of the paper based on which this thesis is written.

My sincere appreciation is due to my siblings who inspired me the most and my friends who have been always there for me.

TABLE OF CONTENTS

Page

TABLE OF CONTENTS

EXAMINATION COMMITTEE PAGE 2

COPYRIGHT PAGE 3

ABSTRACT 4

ACKNOWLEDGEMENTS 6

LIST OF ABBREVIATIONS 9

LIST OF ILLUSTRATIONS 10

LIST OF TABLES 11

Chapter 1: Introduction 12

Chapter 2: Experimental Setup 17

Chapter 3: Results and Discussion 20

3.1 In-Cylinder Pressure 21

3.2 P-V Diagrams 24

3.3 In-Cylinder Gas Temperature 28

3.4 Heat Release Rate 30

3.5 Emissions Analysis 36

3.6 Efficiency Analysis 41

3.6.1 Combustion Efficiency 45

3.6.2 Gas Exchange Efficiency 46

3.6.3 Thermodynamic Efficiency 48

3.6.4 Indicated Thermal Efficiency 51

Chapter 4: Conclusions 53

BIBLIOGRAPHY 56

Appendices 59

Appendix A: Fourier Transform Infrared Analyzer 59

Appendix B: Accuracy and Repeatability 61

LIST OF ABBREVIATIONS

aTDC	After top dead center
CA50	Crank angle degree at which 50% of heat is released
CAD	Crank angle degree
CFR engine	Cooperative fuel research engine
CLMEP	Combustion losses mean effective pressure
EXMEP	Exhaust losses mean effective pressure
FTIR	Fourier transform infrared
FuelMEP	Supplied fuel energy
HCCI	Homogenous charge compression ignition
HTMEP	Heat transfer losses mean effective pressure
IMEP	Indicated mean effective pressure
LHV	Lower heating value
PMEP	Pumping losses mean effective pressure
QMEP	Released heat mean effective pressure
R_c	Compression ratio
RON	Research octane number
TDC	Top dead center
UHC	Unburned hydrocarbons

LIST OF ILLUSTRATIONS

Figure 1: Schematic of the experimental setup. 19
Figure 2: In-cylinder pressure traces for λ = 4, uncooled (orange) and cooled (blue). 22
Figure 3: In-cylinder pressure traces for λ = 5, uncooled (orange) and cooled (blue). 24
Figure 4: In-cylinder pressure vs volume for λ = 4, uncooled (orange) and cooled (blue). 25
Figure 5: Enlarged view of the in-cylinder pressure vs volume diagram capturing the negative work for λ = 4, uncooled (orange) and cooled (blue). 26
Figure 6: In-cylinder pressure vs volume for λ = 5, uncooled (orange) and cooled (blue). 27
Figure 7: Enlarged view of the in-cylinder pressure vs volume diagram capturing the negative work for λ = 5, uncooled (orange) and cooled (blue). 28
Figure 8: In-cylinder temperature vs CAD for λ = 4, uncooled (orange) and cooled (blue). 29
Figure 9: In-cylinder temperature vs CAD for λ = 5, uncooled (orange) and cooled (blue). 30
Figure 10: Model of specific heat ratio, γ, as a function of temperature plotted against corresponding CAD for all cases. 33
Figure 11: Heat release rate for λ = 4, uncooled (orange) and cooled (blue). 34
Figure 12: Heat release rate for λ = 5, uncooled (orange) and cooled (blue). 36
Figure 13: Specific emissions and concentration of unburned hydrocarbons (UHC) in the exhaust for all cases 38
Figure 14: Specific emissions and concentration of carbon monoxide (CO) in the exhaust for all cases. 39
Figure 15: Specific emissions and concentration of nitrogen oxides (NOx) in the exhaust for all cases. 40
Figure 16: FuelMEP breakdown by percentage for all cases. 41
Figure 17: Combustion efficiency for all cases. 45
Figure 18: Gas exchange efficiency for all cases. 47
Figure 19: Thermodynamic efficiency for all cases. 50
Figure 20: Indicated thermal efficiency for all cases. 52
Figure 21: FTIR Infrared Spectrum 59
Figure 22: PT diagram for n-heptane at different intake temperatures [25] 62
Figure 23: PT diagram for primary reference fuel 60 at different intake temperatures [25]. 63
Figure 24: PT diagram for primary reference fuel 90 at different intake temperatures [26]. 64

LIST OF TABLES

Table 1: General specifications of the used CFR engine. 17
Table 2: Summary of testing conditions 20
Table 3: The values of IMEPg and QMEP for all cases 49

Chapter 1: Introduction

Recent strict emissions regulations call for more efficient combustion engines now more than ever. Improving the heat engine's efficiency and using technologies that have better emissions control have been of major interest as they can help meet these environmental regulations. The brake efficiency of an engine can be expressed as the lumped efficiency (product) of four other efficiencies, namely: combustion efficiency (associated with energy lost in the form of incomplete combustion), thermodynamic efficiency (thermodynamic cycle's efficiency of heating the charge, expanding hot gasses, and producing work), gas exchange efficiency (associated with energy lost in replacing the burned charge with a fresh one), and mechanical efficiency (associated with friction losses). It has been reported in the literature that the combustion efficiency, gas exchange efficiency, and mechanical efficiency can reach values as high as 99.9%, 104% (turbocharged), and 95%, respectively [1–3].

On the contrary to the other types of efficiencies, researchers have been struggling to improve the typically low thermodynamic efficiency (compared to other efficiencies) but their efforts have been in vain and to the best of the authors' knowledge, one of the highest reported values is 55% [4]. Thus, thermodynamic efficiency remains the main obstacle facing the achievement of high brake efficiency. One of the main guidelines used in research to improve the thermodynamic efficiency is the ideal Otto cycle. The cycle starts with isentropic compression, then isochoric heat addition, followed by isentropic expansion, and finally, isochoric heat subtraction. Otto cycle predicts that

running the engine at high compression ratios and using working fluids with relatively high specific heat ratio in the combustion reaction are the two factors that can improve the thermodynamic efficiency which is described by the relation: $\eta_{TH,Otto} = 1 - {1}/{R_c^{\gamma-1}}$, where R_c is the compression ratio and γ is the specific heat ratio of the working fluid.

Many approaches have been introduced in the engines research community in order to improve the thermodynamic efficiency of combustion engines. One of the main examples of such technologies is the homogeneous charge compression ignition (HCCI). HCCI is typically run with lean fuel/air mixtures to limit its typically high combustion rate caused by the ignition onset occurring simultaneously in multiple locations in the cylinder [5]; this gives the opportunity of running the engine at high compression ratios without generating intense knock (pressure waves produced by the undesired auto ignition of end gasses that can damage the engine). Furthermore, since air has higher specific heat ratio than common fuels, the weighted average of the specific heat ratio increases when using lean fuel/air mixtures which is the case in HCCI and so this should improve the thermodynamic efficiency. In addition, the typically low-temperature combustion in HCCI leads to less NO_x formation in the emissions. Indeed, when HCCI was compared with SI mode in terms of indicated efficiency and NO_x formation, HCCI was the better choice in both aspects [6]. The multi-fuel, multi-compression-ratios flexibility of HCCI has been studied in number of publications and it was shown that it can be run with wide range of fuels and compression ratios [7]. Furthermore, the cycle-

to-cycle variation in the produced work in HCCI is very small [8] which is attributed to the uniform, simultaneous combustion at multiple locations in the cylinder in HCCI mode [9]. All of the aforementioned reasons make the HCCI a very good candidate in terms of achieving high thermodynamic efficiency with minimal NO_x emissions.

The second factor affecting the thermodynamic efficiency in the ideal Otto cycle is the specific heat ratio to which there was not much attention paid by researchers compared to the compression ratio factor, mainly due to the feasibility of varying it. However, the noble-gas power cycle was introduced to investigate the specific heat ratio factor. The main concept of the cycle is to replace air in combustion processes with oxygen-noble-gas mixture. The selection of noble gasses as a dilution was based on two factors: 1) they have a significantly higher specific heat ratio (=1.67) than that of air (=1.4), and 2) they have very low chemical reactivity which means that they will only work as a dilution in the combustion reaction and will not take part in forming any NO_x or other emissions, i.e., NO_x are eliminated from the combustion products. Hence, the noble gas can be rerouted back from the exhaust to the intake which makes the idea sustainable. If the elimination of CO_2 is to be achieved, hydrogen can be used as a fuel in which case, the exhaust gasses would consist of only water and the noble gas [10–12]. The most common noble-gas power cycle is the argon power cycle. In 1978, Laumann et al. first suggested this idea as a US patent and accompanied it with the use of hydrogen as a fuel [13]. Multiple studies were conducted to test the feasibility and benefits of this power cycle on thermal efficiency and emissions. It was concluded that due to intense

knock occurrence, it is very difficult to apply the argon power cycle at stoichiometric ratios (here stoichiometry is defined based on the fuel/oxidizer ratio). Furthermore, it was found that using the hydrogen-oxygen-argon cycle can obtain a thermal efficiency of 50% in a CFR SI engine with high concentration of argon [14–16]. Similar findings were published on a CI engine run using hydrogen-oxygen-argon cycle [17].

The idea of combining the HCCI mode with argon power cycle in order to combine the effects of running at high compression ratios and high working fluid's specific heat ratio, seems appealing. In fact, Mohammed et al. investigated the advantages of such a combination by comparing it with an air-breathing engine. However, a major problem that faced that study was the intense knock caused by the high in-cylinder temperature caused by argon. The intense knock made it difficult to further increase the compression ratio which is desired if the full potential of the argon cycle in HCCI were to be fully realized. Hence, the high in-cylinder temperatures caused by the use of argon counteracted the advantage of the low in-cylinder temperatures typically obtained in HCCI which enable the engine of running at high compression ratios without too intense knock. In that study, the fuel-air mixture was run at R_c = 15 and the fuel-oxygen-argon mixture was run at R_c = 8.8 and interestingly enough, the fuel-oxygen-argon mixture achieved slightly higher thermal efficiency; this shows the cancellation effect of the low compression ratio against the high specific heat ratio on the thermal efficiency. This cancellation effect limits our perception of the full potentials of combining the two technologies [18].

This study investigates the potentials of combining the HCCI mode with the argon power cycle at high compression ratios. The problem of knock that was previously faced at high compression ratio was mainly solved by cooling the intake charge to subzero temperatures which lowered the in-cylinder temperature and counteracted the effect of increasing the compression ratio on the combustion phasing and indeed, made it possible to increase the compression ratio up to 15.2. Furthermore, a highly resistive fuel to auto ignition was used, which is pure methane with RON = 120. It should be noted that the concept of argon power cycle accompanied with cooling is more applicable in stationary power plants where cooling can be done through several techniques and the separation of argon from the emissions can be achieved with re-routing the argon back to the intake. Results compare uncooled cases corresponding to relatively low knock-limited compression ratios and cooled cases corresponding to relatively high knock-limited compression ratios. The breakdown of fuel's energy into different energy losses is provided to better understand the efficiencies' results. Results show that cooling the intake charge resulted in less complete combustion (more UHC and CO emissions) and so slightly lower combustion efficiency. Furthermore, cooling the intake decreased the intake pressure which resulted in lower gas exchange efficiency. As for the thermodynamic efficiency, it was found that heat losses dictated the improvement of it and overall, it remained almost unchanged. As a result of all of this, the indicated thermal efficiency slightly decreased in the cooled-high-compression-ratios cases. However, in general, the obtained indicated thermal efficiency values for all cases are relatively high with maximum of 48.3%.

Chapter 2: Experimental Setup

A standard Waukesha single cylinder variable compression ratio CFR engine was used to conduct all the experiments. Some modifications were made on the engine to allow to operate in the HCCI mode; it, originally, was equipped with a carburetor set upstream relative to the intake valve. Since the carburetor was designed to operate under stoichiometric or almost stoichiometric air/fuel mixtures, it was replaced with a port fuel injector set adjacent to the intake valve to enable the engine to run under both stoichiometric conditions and very lean conditions which is required for running the HCCI mode. Table 1 summarizes the specifications of the used CFR engine.

Table 1: General specifications of the used CFR engine.

Parameter	Value
Displaced volume [cc]	611.7
Stroke [mm]	114.3
Bore [mm]	82.55
Connecting rod [mm]	256
Compression ratio Rc	4 to 18
Number of valves	2
Exhaust valve opening [CA ATDC]	140
Exhaust valve closure [CA ATDC]	-345
Inlet valve opening [CA ATDC]	-350
Inlet valve closure [CA ATDC]	-146
Coolant water temperature [℃]	100 ± 1.5
Oil temperature [℃]	57 ± 8

The gases used in this experiment were argon, oxygen and pure methane (CH4), whose flows were controlled by Brooks mass flow controllers with an accuracy of ± 0.5 % of the flow rate and ± 0.1 % of the full scale (1000 slpm). Pure methane was chosen as a fuel for this study since one of the main targets is to maximize the compression ratio, and pure methane has a RON = 120 which indicates that it has a high resistance to auto-ignition and so, high compression ratios can be reached without having severe knock.

Instead of the standard detonation pickup sensor, a QC34D AVL pressure transducer, set on one side of the combustion chamber, with an accuracy of ±0.3% of the full scale (150 bar) was used to measure the in-cylinder pressure. The signal digitized in an A/D converter is amplified using a charge amplifier. Two AVL LP11DA absolute pressure transducers, set on each port with an accuracy of ±0.1% of the full scale (0 to 10 bar), were used to record the intake and exhaust pressures as a function of crank angle. The values of these two pressures were acquired with the aid of an AVL 365C encoder that had a resolution of 0.2 crank angle. Hence, each cycle consisted of 3600 measurements. As for the intake and exhaust temperatures, they were measured using K-type thermocouples with an accuracy of ±2 K. Finally, the results were acquired and averaged over 200 recorded consecutive cycles.

An AVL SESAM i60 FTIR analyzer was used to measure the concentration of emissions in the exhaust. The analyzer is equipped with a built-in software which provides the concentration of 25 different exhaust species. Figure 1 illustrates a schematic of the experimental setup.

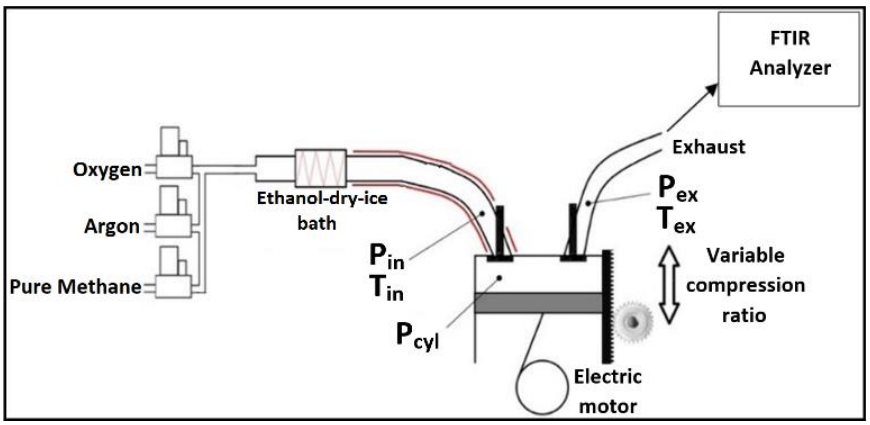

Figure 1: Schematic of the experimental setup.

The flows were dictated by the following parameters: 1) required oxygen/methane equivalence ratio (λ = 4 and λ = 5), 2) intake pressure, which was to be kept at 1.02±0.05 bar, and 3) the ratio $\frac{\text{argon flow}}{\text{argon flow} + \text{oxygen flow}}$ which was to be kept as 0.79 to mimic the volumetric ratio of nitrogen in air.

The equivalence ratio, λ, in this study is defined as $\frac{\left({}^{\text{oxygen}}/_{\text{fuel}}\right)_{\text{exp}}}{\left({}^{\text{oxygen}}/_{\text{fuel}}\right)_{\text{st}}}$. The intake temperature was cooled via an ethanol-dry-ice bath used as a heat exchanger. All gasses were passed through coiled copper pipes which were submerged into the heat exchanger bath before reaching the intake manifold. The combustion was fairly stable throughout all the experiments. Readings were repeated for at least three times and there was not any considerable fluctuation in them. Table 2 summarizes the testing conditions.

Table 2: Summary of testing conditions

Parameter	Value
Rotation speed [rpm]	600
Intake temperature [℃]	-6.0, 40.0 (±1.0)
Intake pressure [bar]	1.07 bar for uncooled and 0.97 bar for cooled
Equivalence ratio, λ	4, 5
Fuel	Pure methane

Chapter 3: Results and Discussion

The effects of two main variables on the thermal efficiency are investigated in this thesis, namely, the intake temperature and the oxygen-fuel equivalence ratio, λ. The intake temperature is of interest here since cooling the intake, indeed, enabled us to test higher compression ratios with minimal knock intensity and this theoretically should increase the thermodynamic efficiency. Therefore, the readings were taken at maximum possible compression ratios at which the knock intensity was too high (dP/dCAD ~ 15 bar/CAD) to further increase the compression ratio. For this purpose, two intake temperatures were investigated, which are: Tin = 40 °C (the uncooled case which corresponded to relatively lower knock-limited-Rc; the exact values are shown in the next section) and Tin = -6.0 °C (the cooled case which corresponded to relatively higher knock-limited-Rc; the exact values are shown in the next section). As for the oxidizer-fuel equivalence ratio, λ = 4 and λ = 5, were investigated. The reason for this variation is to capture the effect of combustion phasing on the results; that is, since for λ = 4 the

combustion phasing was very late at the knock-limited compression ratio, the only way to shift the combustion phasing earlier for the same operating conditions, was to test a leaner charge with higher Rc, which indeed, shifted the combustion phasing to a fairly acceptable range. Thus, in total, we have four cases; case 1: uncooled λ = 4, case 2: cooled λ = 4, case 3: uncooled λ = 5, and case 4: cooled λ = 5. The main comparisons will be based upon varying the intake temperature (and corresponding compression ratios) and fixing the oxidizer-fuel equivalence ratio.

3.1 In-Cylinder Pressure

Figure 2 illustrates the in-cylinder pressure trace for λ = 4, both cooled and uncooled vs crank angle degree. Although achieving identical combustion phasing here was not taken into account while conducting the experiment since the main target was to have the maximum possible compression ratio, the two in-cylinder pressure traces show that combustion onsets for the two cases were very close which will be shown in the heat release rate results. This is due to the fact that cooling the intake in HCCI shifts the combustion phasing to later CADs (retards the combustion phasing) while increasing the compression ratio shifts the combustion phasing to earlier CADs (advances the combustion phasing). Thus, the two effects counteracted each other, and we are left with almost the same phasing. This is an important aspect of cooling the intake since having too early combustion phasing (before TDC) yields negative work on the piston.

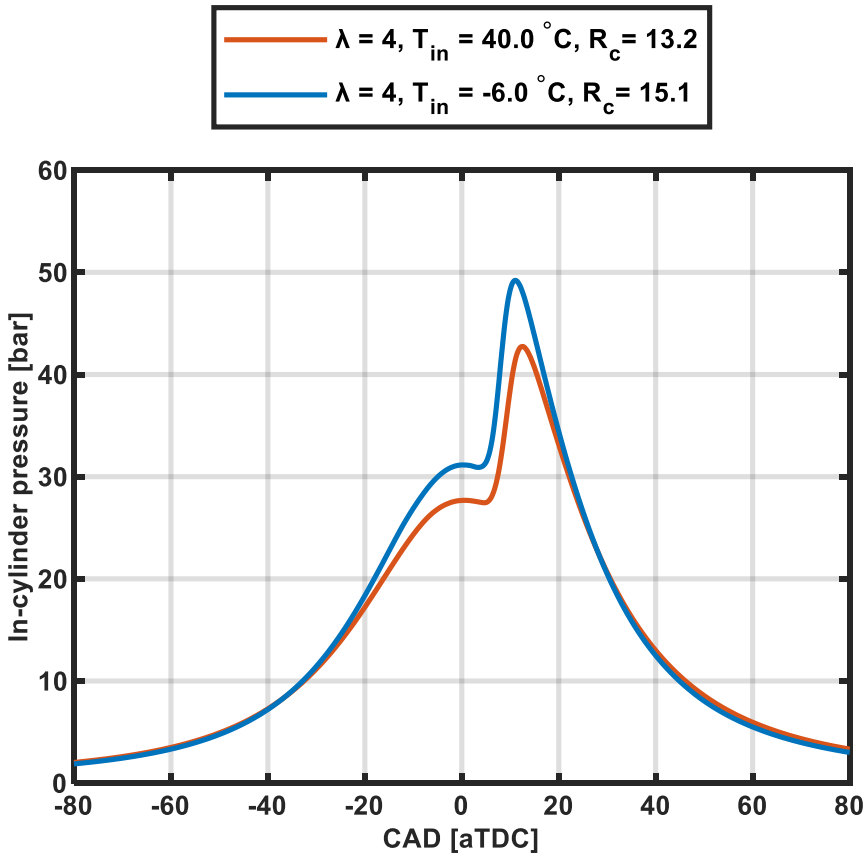

Figure 2: In-cylinder pressure traces for λ = 4, uncooled (orange) and cooled (blue).

As expected, the cooled case that achieved higher compression ratio has globally higher in-cylinder. This behavior can be explained by the following equations of isentropic compression:

$$P_2 = P_1 R_c^{\gamma} \qquad (1)$$

$$T_2 = T_1 R_c^{\gamma - 1} \qquad (2)$$

Where the subscripts (1) and (2) denote the states before and after the compression stroke, respectively, and:

P is the in-cylinder pressure.

R_c is the compression ratio.

γ is the specific heat ratio.

T is the in-cylinder temperature.

Figure 3 illustrates the in-cylinder pressure trace for λ = 5, both cooled and uncooled as a function of crank angle degree. As mentioned earlier, the cold intake temperature canceled the effect of increasing the compression ratio on the combustion phasing. Furthermore, the in-cylinder pressure of the lean case (Figure 3) reached higher values than that of the richer case (Figure 2). This could be attributed to the higher compression ratio of the leaner case and the relatively late combustion phasing of the richer case; as will be shown later in the P-V diagrams, the late combustion phasing caused the in-cylinder pressure to drop.

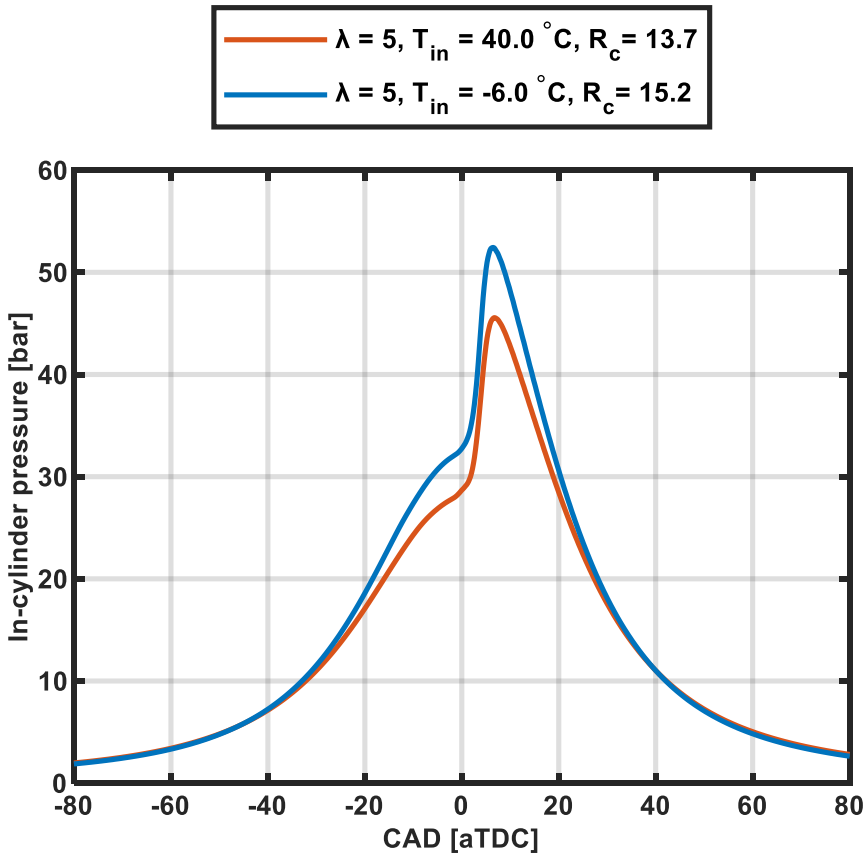

Figure 3: In-cylinder pressure traces for λ = 5, uncooled (orange) and cooled (blue).

3.2 P-V Diagrams

Figure 4 illustrates the pressure-volume diagram for both the uncooled and cooled cases of λ = 4. It is evident from Figure 4 that the cooled case having higher compression ratio was compressed to lower volume than the uncooled case and hence, higher in-cylinder pressure was achieved. Furthermore, heat is added very rapidly and at a constant volume for both cases; this is expected since the complete ignition of the already homogenous charge in HCCI occurs in a very short time compared to other traditional combustion modes such as SI (where the heat release is limited by flame speed) or CI (where the heat release is limited by the mixing of air and fuel). However, the uncooled

case achieved higher in-cylinder pressure than the cooled case at the same volume (for all values of volume > 0.05 L). This will explain later the higher indicated mean effective pressure (IMEP) of the uncooled case. Finally, the absence of low temperature heat release is evident as the pressure only increases dramatically once at the main heat release region and no other heat release can be seen.

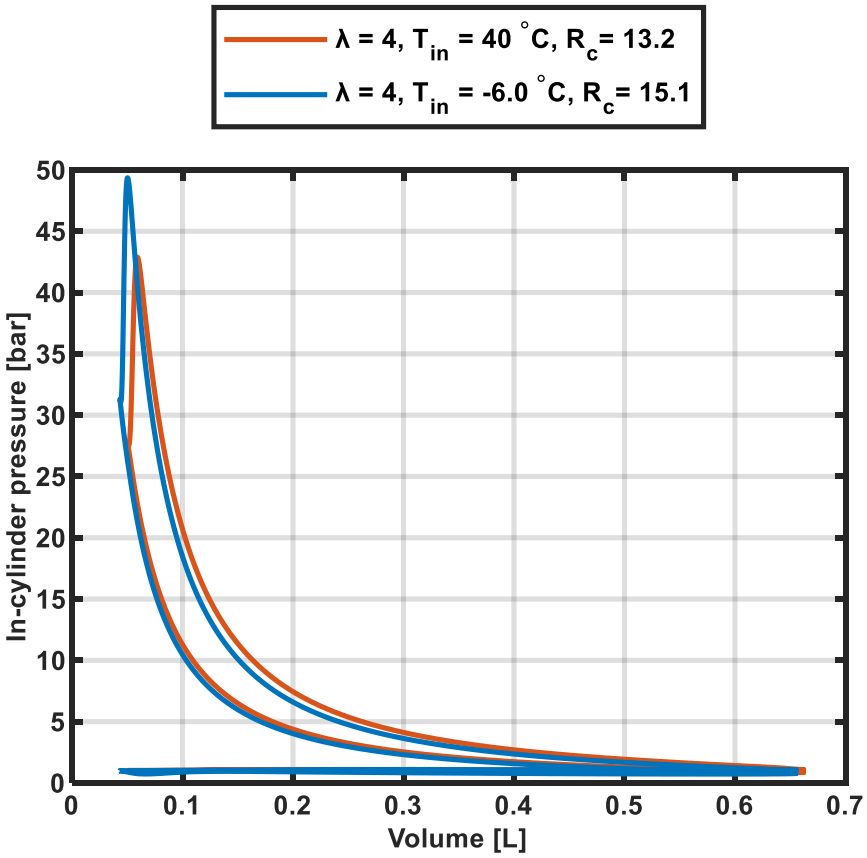

Figure 4: In-cylinder pressure vs volume for λ = 4, uncooled (orange) and cooled (blue).

An enlarged view of interest is shown in Figure 5 in which the negative work of the cycle used in gas exchange is illustrated. Since the cooled charge had lower intake pressure, the work needed to pump out the burned charge and replace it with fresh charge in the cooled case is larger than that needed for the uncooled case. The larger area of the

negative work done in the cooled case explains the difference in gas exchange efficiency and the difference in net indicated mean effective pressures (IMEPn) between the cooled and uncooled cases which will be later shown in this thesis.

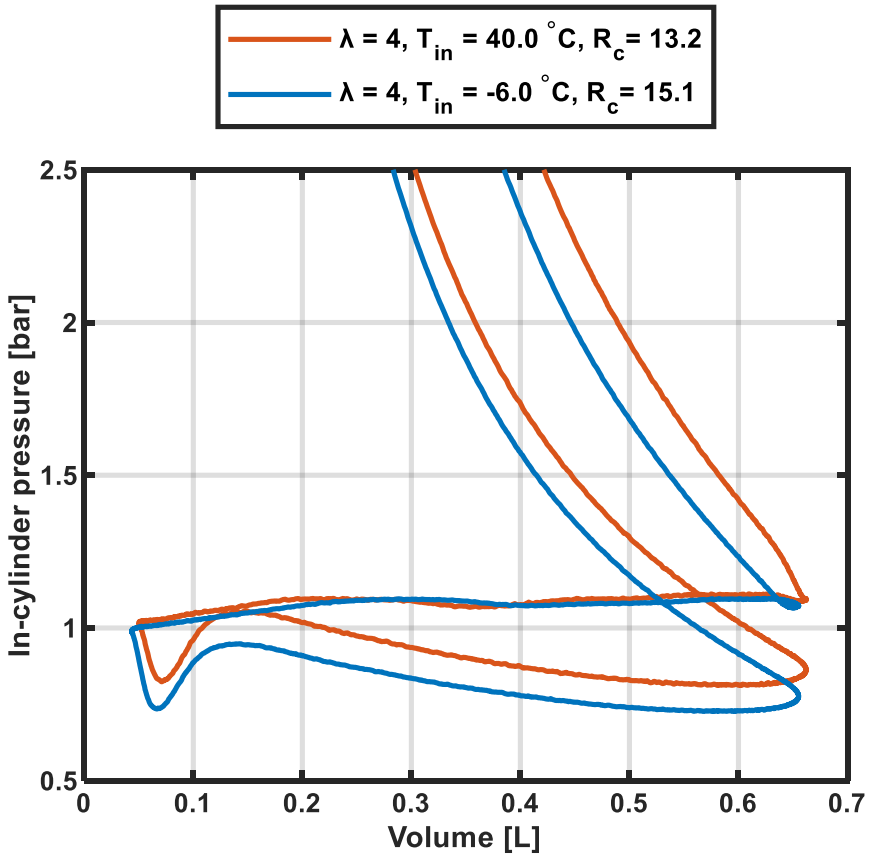

Figure 5: Enlarged view of the in-cylinder pressure vs volume diagram capturing the negative work for λ = 4, uncooled (orange) and cooled (blue).

Figure 6 illustrates the pressure-volume diagram for both uncooled and cooled cases of λ = 5. All findings from Figure 4 apply here but the main difference here is that unlike the previous cases, the curves are smooth at the onset of heat release which makes sense as the combustion phasing in these two cases is earlier than that of the two cases of λ = 4 and so the increase in pressure in Figure 6 started just before expansion.

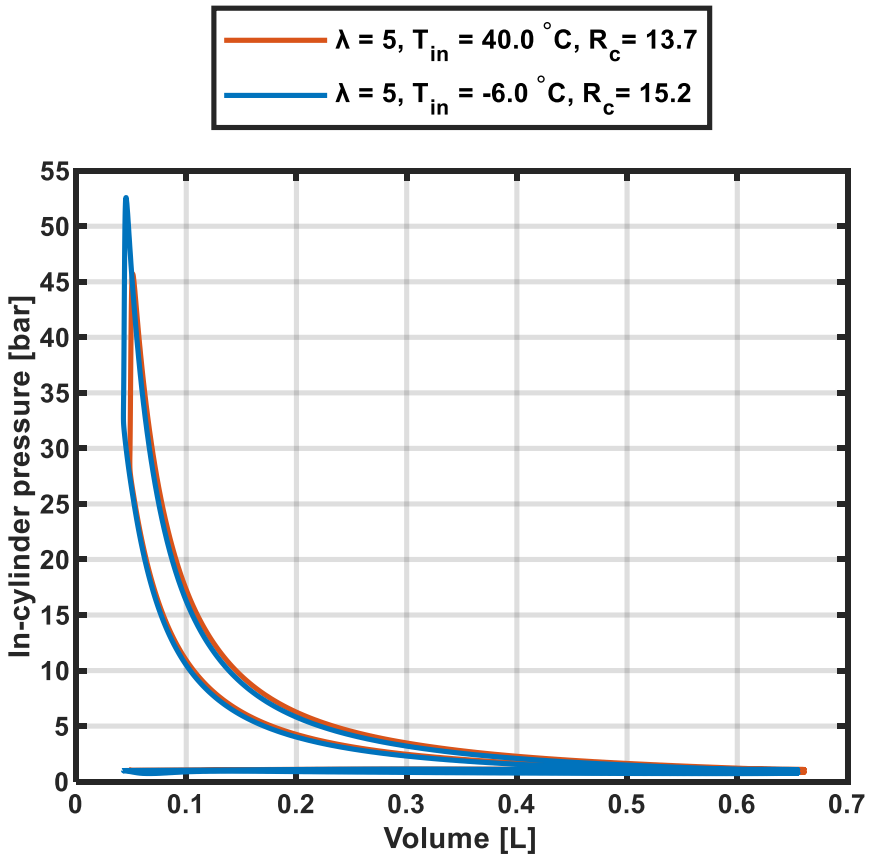

Figure 6: In-cylinder pressure vs volume for λ = 5, uncooled (orange) and cooled (blue).

Figure 7 shows an enlarged view capturing the negative work of the cycle used in gas exchange of the cases of λ = 5. Similar to the two cases of λ = 4, the work done in gas exchange in the cooled case is more than that done in the uncooled case due to the decrease in the intake pressure of the cooled charge.

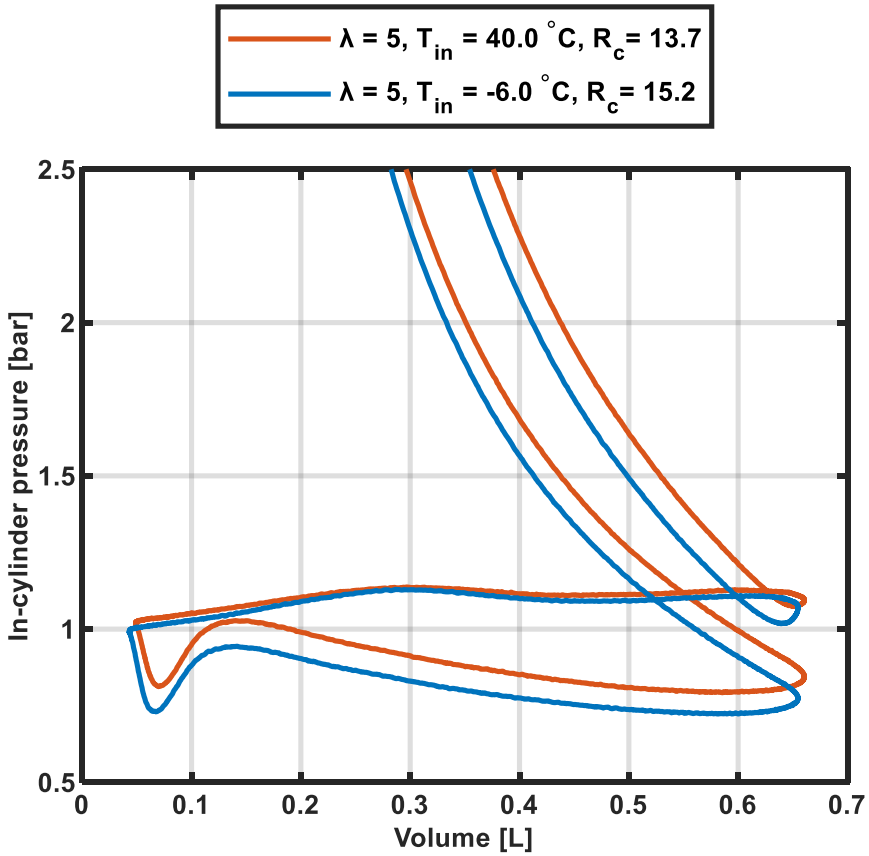

Figure 7: Enlarged view of the in-cylinder pressure vs volume diagram capturing the negative work for λ = 5, uncooled (orange) and cooled (blue).

3.3 In-Cylinder Gas Temperature

In-cylinder temperature is a governing variable in all combustion modes but in HCCI more than any other; this is due to the fact that chemical kinetics govern HCCI, and autoignition occurs only when the right combination of pressure and temperature is met. Figure 8 and Figure 9 illustrate the in-cylinder temperature vs CAD for λ = 4 and λ = 5, respectively. These temperature profiles were generated from the measured pressure traces using the ideal gas law. One interesting finding is that the maximum in-cylinder temperatures for the two cases of λ = 4, shown in Figure 8, are higher than those of λ =

5, shown in Figure 9. This could be attributed to the fact that more fuel means more energy and less dilution and so higher temperature. Furthermore, as expected, the maximum in-cylinder temperatures of the uncooled cases are higher than those of the cooled cases. The effect of this low-temperature combustion on the emissions will be discussed later in this thesis.

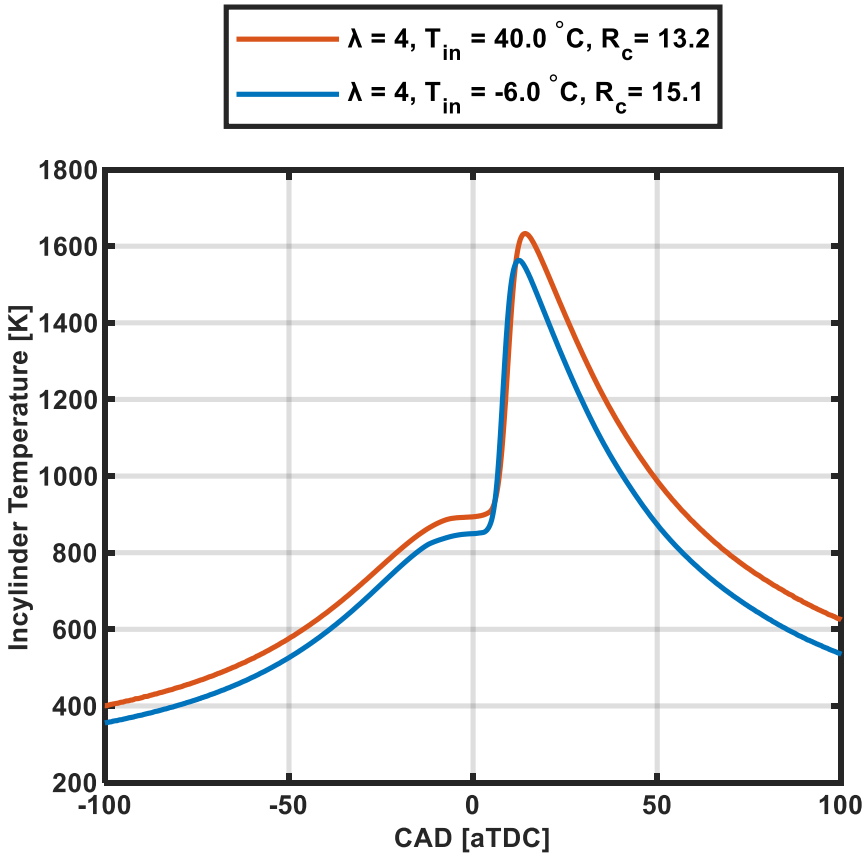

Figure 8: In-cylinder temperature vs CAD for λ = 4, uncooled (orange) and cooled (blue).

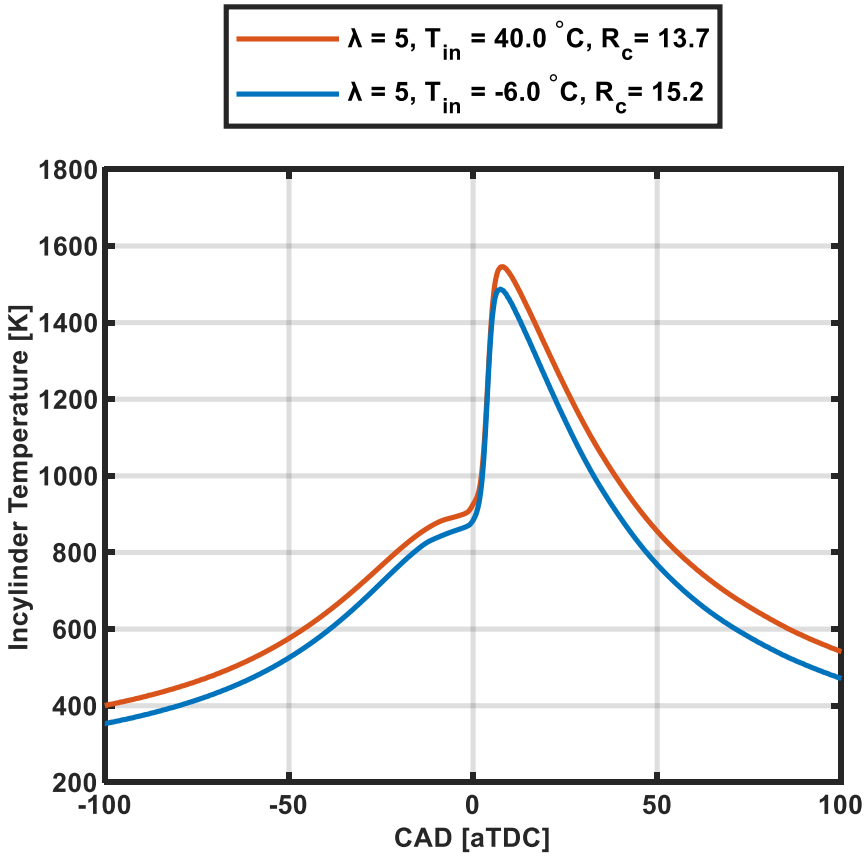

Figure 9: In-cylinder temperature vs CAD for λ = 5, uncooled (orange) and cooled (blue).

3.4 Heat Release Rate

Ideal gas law together with the first law of thermodynamics are used to estimate the heat release rate (ignoring crevices' losses) as follows:

$$dQ_{hr} = dU_s + dQ_{ht} + dW \qquad (3.1)$$

Where:

Q_{hr} is the heat release (gross).

U_s is the sensible energy of the charge.

Q_{ht} is the heat transfer losses.

W is the work done by piston.

Substituting the following into (3.1):

$$dU_s = mc_v dT. \quad (3.2)$$

$$dW = pdV. \quad (3.3)$$

$$\gamma = \frac{c_p}{c_v}. \quad (3.4)$$

$$R = c_p - c_v. \quad (3.5)$$

$$Vdp + pdV = mRdT. \quad (3.6)$$

$$(3.7)$$

Where:

m is the mass of the charge.

c_v is the specific heat at constant volume.

T is the in-cylinder temperature.

γ is the specific heat ratio.

c_p is the specific heat at constant pressure.

R is the universal gas constant.

V is the in-cylinder volume enclosed by the piston's movement.

P is the in-cylinder pressure.

and deriving with respect to θ (CAD), it follows:

$$\frac{dQ_{hr}}{d\theta} = \frac{\gamma}{\gamma - 1} p \frac{dV}{d\theta} + \frac{1}{\gamma - 1} V \frac{dp}{d\theta} + \frac{dQ_{ht}}{d\theta} \qquad (4)$$

This model of heat release rate assumes that the dominant losses are the heat transfer losses and thus, it does not take blow-by nor crevice losses into account. Woschni's heat transfer model was used to estimate the heat losses from the in-cylinder pressure [19].

Since specific heat ratio, γ, is a function of temperature, and since the in-cylinder temperature is changing dramatically throughout the combustion process, it is not reasonable to consider it a constant property. Instead, it was estimated as a function of in-cylinder temperature using NASA's polynomials for calculating heat capacity [20] and the required coefficients were obtained from [21]. To do so, it was assumed that complete combustion took place at once (i.e. all reactants became products at the respective peak pressure of each case). Since the combustion mode is HCCI, it is valid to assume that the charge is instantaneously ignited as the combustion is not dependent on flame propagation as in SI nor mixing of fuel and oxygen as in CI. The combustion duration (CA90-CA10) was roughly 9 CAD (2.5 ms) in all cases which is considerably lower than a typical combustion duration for CI and SI engines. Figure 10 illustrates the profile of this gamma model for all cases as a function of CAD and it is evident that it is changing dramatically during the combustion process, especially, at maximum temperature, and so indeed, considering γ as a constant would not have been a good approximation.

This Gamma model, also, shows that cooling the intake temperature not only will allow higher compression ratios without having sever knock, but also, it slightly increases the specific heat ratio, which as per Otto's ideal cycle, should increase the thermodynamic efficiency.

Finally, the model shows that the leaner the charge is, the higher the specific ratio will be, providing that the flows of oxygen and argon are kept the same, which is the case here. This is expected as argon is the constituent with the highest specific heat ratio among all, and so having more fuel should, indeed, decrease the weighted average of the specific heat ratio.

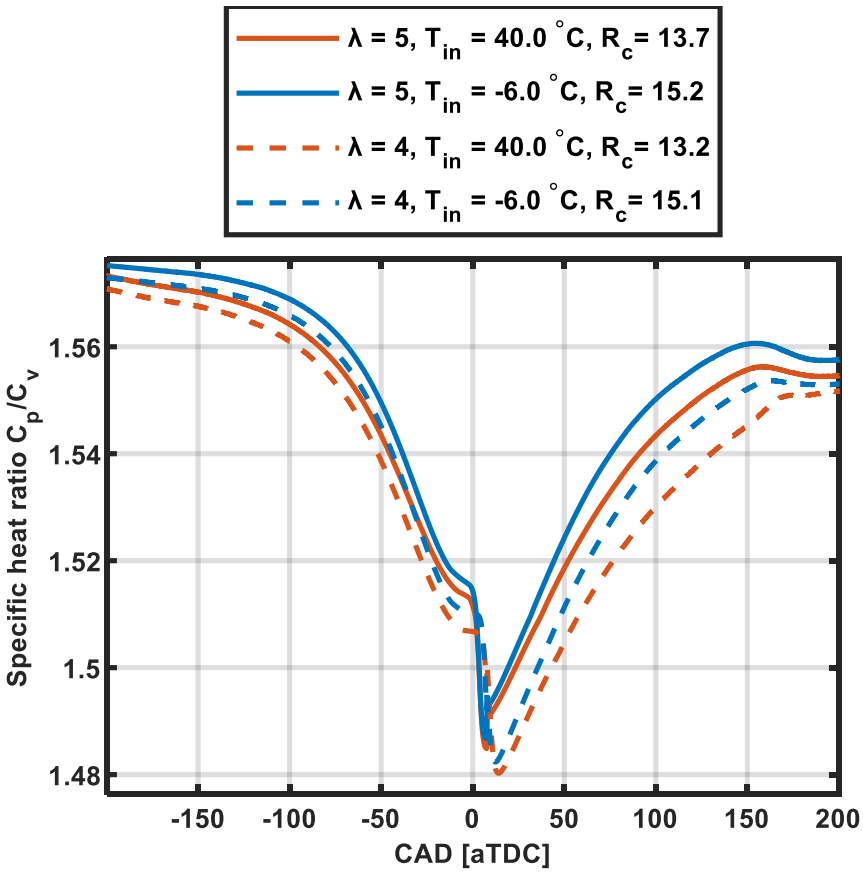

Figure 10: Model of specific heat ratio, γ, as a function of temperature plotted against corresponding CAD for all cases.

Applying equation (4) and using the aforementioned gamma model, the heat release rate was obtained as shown in Figure 11 and Figure 12 for λ = 4 and λ = 5, respectively.

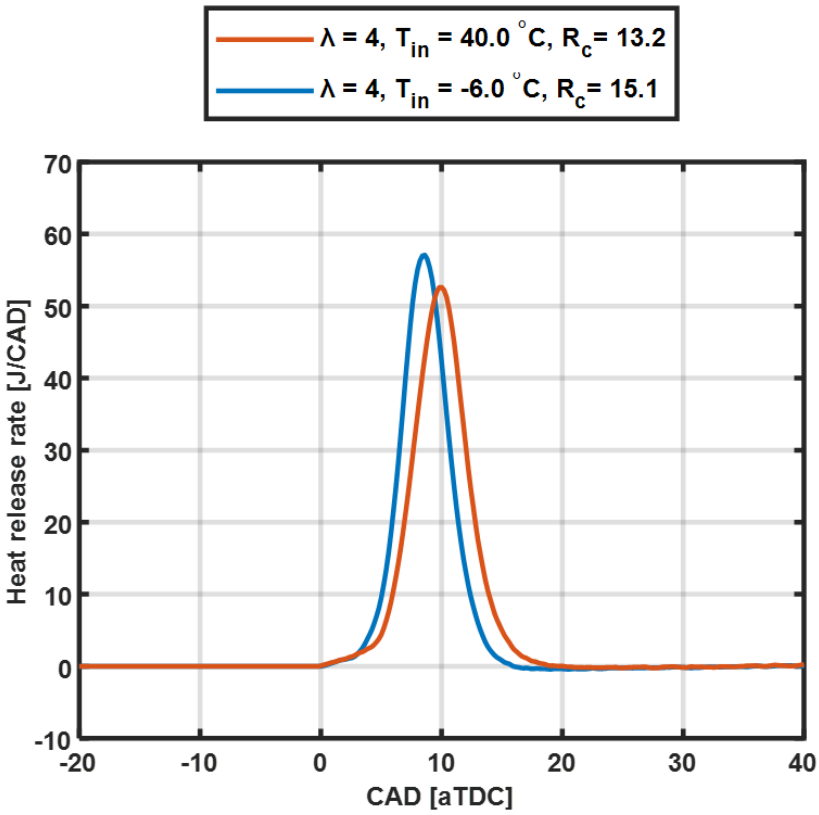

Figure 11: Heat release rate for λ = 4, uncooled (orange) and cooled (blue).

Figure 11 verifies what is earlier mentioned in the in-cylinder pressure section about the combustion phasing of the two cases; that is, the onset of the main combustion of the two cases occurred at very close CADs. This is attributed to the low intake temperature's effect on the combustion phasing almost cancelling the effect of the high compression ratio. It, also, shows that the combustion phasing of the two cases is relatively late (CA50 ~ (9-11) CA aTDC) which was a limitation of the experiment as the knock intensity

was too high to further increase the compression ratio if earlier phasing was to be obtained.

Referring to equation (4), it comes as no surprise that the cooled case with higher compression ratio, and hence, higher maximum in-cylinder pressure yielded higher maximum heat release rate than the uncooled case. Furthermore, as the used fuel was methane which is very resistant to auto ignition with RON = 120, there is no presence of low temperature heat release.

Figure 12 shows that what is mentioned about the cases of $\lambda = 4$, shown in Figure 11, regarding the cooled case achieving higher heat release rate also applies for the two cases of $\lambda = 5$. The main difference here is that the leaner charge (Figure 12) was earlier to burn compared to the richer charge (Figure 11). This is due to the higher compression ratios corresponding to the lean cases moving the combustion phasing to earlier CADs. Another difference to point out is that the leaner charge, although having less FuelMEP (energy of fuel normalized by displacement volume), achieved higher heat release rates; heat release rate is not to be confused with the accumulated heat that will be discussed later in this section.

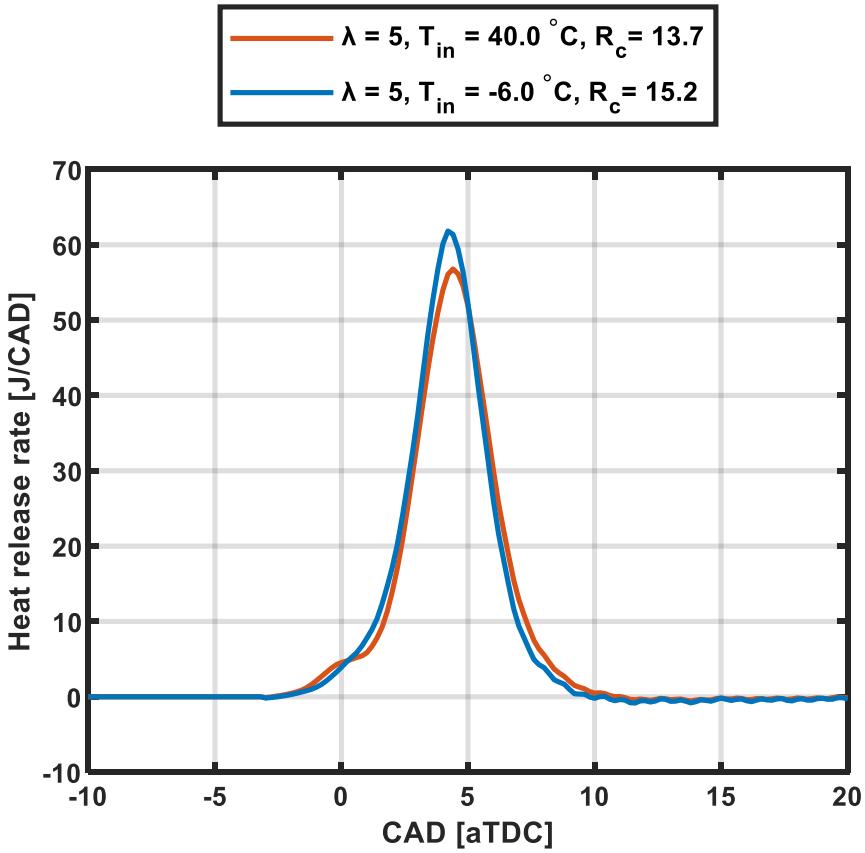

Figure 12: Heat release rate for λ = 5, uncooled (orange) and cooled (blue).

Referring to Figure 2 and Figure 3, it is concluded that the leaner charges (λ = 5) yielded higher maximum in-cylinder pressure than the richer charges (λ = 4). This is reflected on Figure 11 and Figure 12 which show that the heat release rate of the leaner charges reached higher values than that of the richer charges.

3.5 Emissions Analysis

Exhaust analysis is important since it is an indicator of the combustion efficiency. That is, any substance in the products of the combustion reaction having a heating value is considered as an energy loss since an ideal combustion would convert all the chemical

energy into useful work. Exhaust analysis in this study is particularly important as the main variable of the study is temperature which plays a major role in determining the exhaust species and their amounts.

Figure 13 presents the specific emissions and concentration of unburned hydrocarbons (UHC) in the exhaust for all cases. The main trend here is that the lower the temperature is, the more UHC will be in the exhaust. This makes sense as the low in-cylinder temperature hinders the complete combustion of the fuel and so more unburned hydrocarbons are yielded. Of course, the richer charge ($\lambda = 4$) had more UHC in the exhaust than the leaner charge ($\lambda = 5$) as it had more fuel injected.

Another reason explaining the lower-temperature charges yielding more UHC is that the compression ratio of these cases is higher than that of the uncooled cases. Higher compression ratios increase the ratio of the crevice's volume to the compression volume (crevice's volume is the volume between the liner and the piston above the upper piston ring, also known as the top-land volume). This is because the top-land volume does not change with changing the compression ratio, but the compression volume decreases with increasing the compression ratio. This top-land volume gets filled with fuel, which is usually not completely burned and hence, more UHC is yielded. To sum up, lower temperature and higher compression ratios led to more UHC in the emissions. This will be reflected on the combustion efficiency which will be later discussed in this thesis.

It is worth mentioning that a Fourier Transform Infrared (FTIR) analyzer was used to obtain the exhaust emissions. Since the FTIR analyzer does not provide the concentration of the UHC, the following relation that Melo et al. used was utilized for this purpose [22]:

$$UHC = CH_4 + 2C_2H_2 + 2C_2H_4 + 3C_3H_6 + +5IC_5 + 5NC_5 + 7.5AHC \quad (5)$$

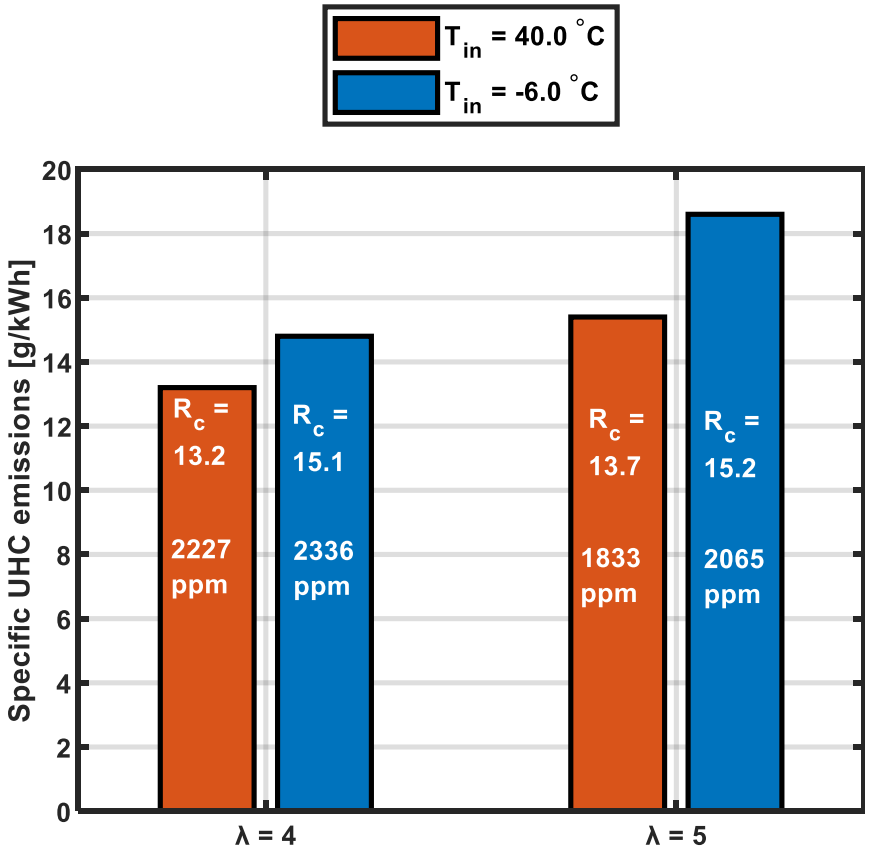

Figure 13: Specific emissions and concentration of unburned hydrocarbons (UHC) in the exhaust for all cases

Figure 14 shows the specific emissions and concentration of carbon monoxide (CO) in the exhaust for all cases. For the oxidation of carbon monoxide (to CO2) to take place, the in-cylinder temperature has to be high enough to provide the required energy for the oxidation process. Otherwise, CO will be present in high concentrations in the exhaust. This explains why the cooled case of λ = 5 yielded more CO than the uncooled case. As for the case of λ = 4, Figure 11 shows that unlike the case of λ = 5, the duration of the combustion in the uncooled case was slightly longer than that of the cooled case and since the oxidation of CO is a relatively slow reaction, this could justify the cooled case producing more CO.

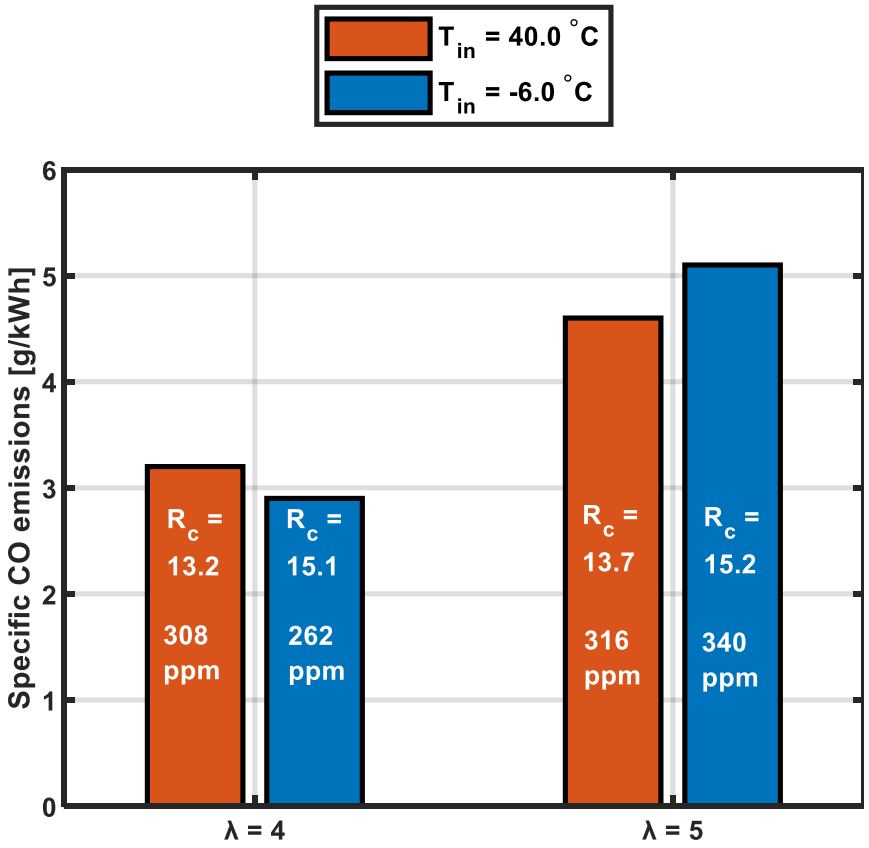

Figure 14: Specific emissions and concentration of carbon monoxide (CO) in the exhaust for all cases

Figure 15 illustrates the specific emissions and concentration of nitrogen oxides (NOx) in the exhaust for all cases. Although nitrogen was not part of the reactants in any of the cases, some insignificant amounts of (NOx) were detected by the FTIR analyzer. This could be attributed to the nitrogen impurities present in the argon and oxygen gas cylinders. The evident trend is that the cooled cases yielded less NOx as the temperature was not high enough to activate the formation of high amount of NOx from the nitrogen impurities in the gas cylinders.

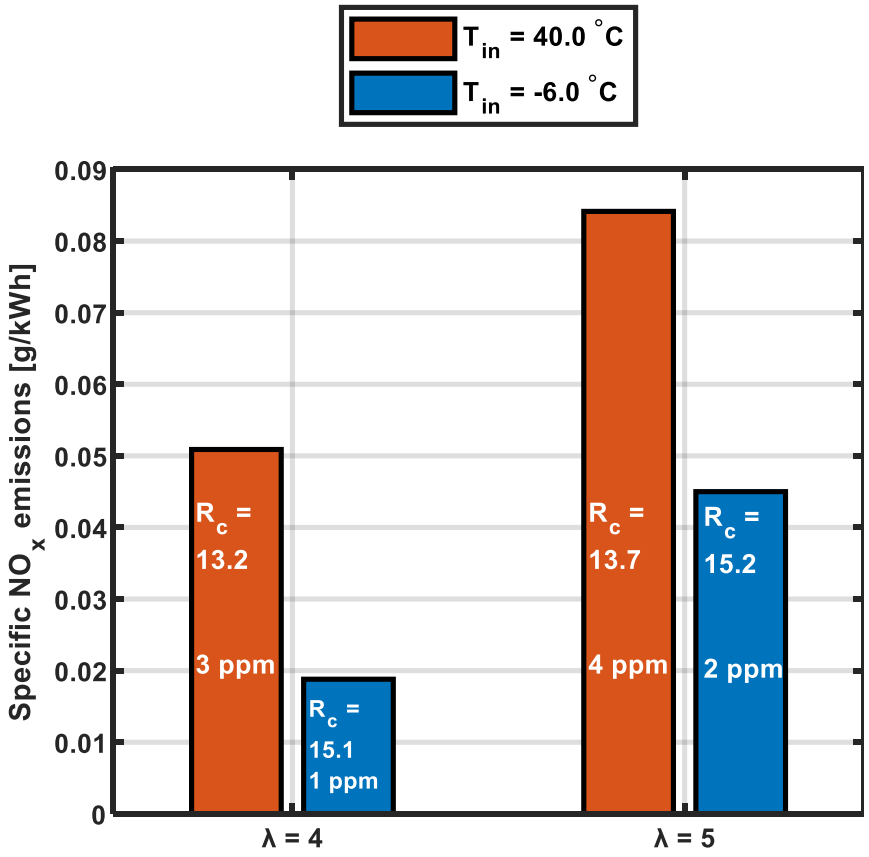

Figure 15: Specific emissions and concentration of nitrogen oxides (NOx) in the exhaust for all cases

3.6 Efficiency Analysis

Figure 16 shows the FuelMEP breakdown by percentage into five components, one of which is the net work produced by the thermodynamic cycle (net indicated mean effective pressure, IMEPn) and the other four are energy losses. Hence, the sum of all five components is equivalent to FuelMEP. This breakdown will help understand the values of different efficiencies that will be discussed later in this section.

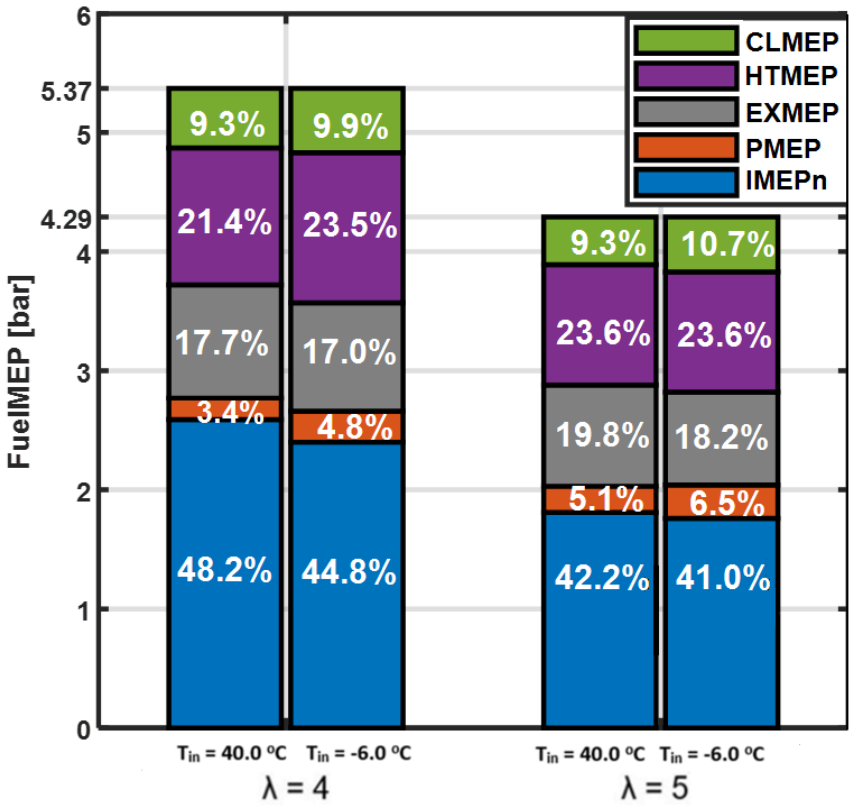

Figure 16: FuelMEP breakdown by percentage for all cases.

Indicated mean effective pressure, IMEPn, is, by definition, the total area enclosed by the P-V diagram divided by the displacement volume as shown in equation (6):

$$IMEP_n = \frac{1}{V_D}\int_0^{720} pdV \qquad (6)$$

Where:

V_D is the displacement volume.

So, IMEPn accounts for both the positive work and the negative work done to replace the burned charge with a fresh one. Referring to Figure 4 and Figure 6 corresponding to the P-V diagrams of the cases of λ = 4 and λ = 5, respectively, it is evident that the positive work area of the cooled and uncooled cases are very close to each other, except for the region where V < 0.05 L that only could be reached with higher compression ratio. However, referring to Figure 5 and Figure 7 which focus on the negative work area, one can see that the negative work done by the cooled charge is larger than that done by the uncooled one. This could be attributed to the cooled charge having lower intake pressure and so more work is needed to replace the burned charge with a fresh one. This explains why IMEPn dropped for both cases when the intake temperature of the charge is decreased. The same reasoning explains the values of the pumping mean effective pressure, PMEP, which can be defined as the aforementioned negative work divided by the displacement volume.

EXMEP is the exhaust losses which can be approximated as follows:

$$EXMEP = \frac{mc_p(T_{exh} - T_{amb})}{V_D} \qquad (7)$$

Where:

m is the mass of the products.

c_p is the heat capacity at constant pressure.

T_{exh} is the exhaust temperature.

T_{amb} is the ambient temperature.

Equation 7 gives an approximation and not the exact value since T_{exh} here is time averaged and not mass averaged. Since there was not much variation in T_{exh}, this should be a good estimation. Since the cooled charges had lower T_{exh}, EXMEP decreased for the cooled cases.

Heat losses mean effective pressure, HTMEP was calculated using the following equation:

$$HTMEP = QMEP - EXMEP - IMEP_n - PMEP \qquad (8)$$

Where $QMEP$ is the amount of heat released divided by the displacement volume and it can be calculated using the combustion efficiency which will be discussed later. It is worth mentioning that HTMEP here includes blow-by and crevices losses. Heat losses are mainly affected by three factors, namely, the compression ratio (area-to-volume ratio), the in-cylinder temperature, and the heat transfer coefficient. Increasing the compression ratio increases the combustion chamber's surface-area-to-volume ratio at top dead center, which in turn, increases the heat transfer losses. Furthermore, higher

compression ratios lead to higher in-cylinder pressure and in-cylinder temperature, which in turn, increase the heat losses to the cylinder's wall. Lower in-cylinder temperature, on the other hand, decreases heat transfer losses to the cylinder's wall as the temperature difference is less. As the two effects of higher compression ratio and lower intake temperature are accompanied in this study, the two effects counteract each other. The effect of the heat transfer coefficient will be later addressed in the thermodynamic efficiency analysis.

CLMEP is the combustion losses mean effective pressure. It represents the losses which are in the form of any product of the combustion reaction having a heating value as its chemical energy could have been converted to work. It was calculated as follows:

$$CLMEP = \frac{\sum m_i Q_{LHV,i}}{V_D} \qquad (9)$$

Where:

m_i is the mass of species i in the exhaust which can be known from the concentration measured by the FTIR analyzer.

$Q_{LHV,i}$ is the lower heating values of species i in the exhaust.

Referring to Figure 13, one can see that the UHC increased with lowering the temperature and increasing the compression ratio. The reasons behind this were explained in detail in the discussion of Figure 13. This increase in UHC explains the increase in CLMEP for the cooled charges for both cases as can be seen in Figure 16.

3.6.1 Combustion Efficiency

Figure 17 shows the combustion efficiency of all cases. Combustion efficiency can be thought of as the complementary percentage of the CLMEP/FuelMEP ratio. Therefore, the points raised in CLMEP analysis explain the values shown in Figure 17.

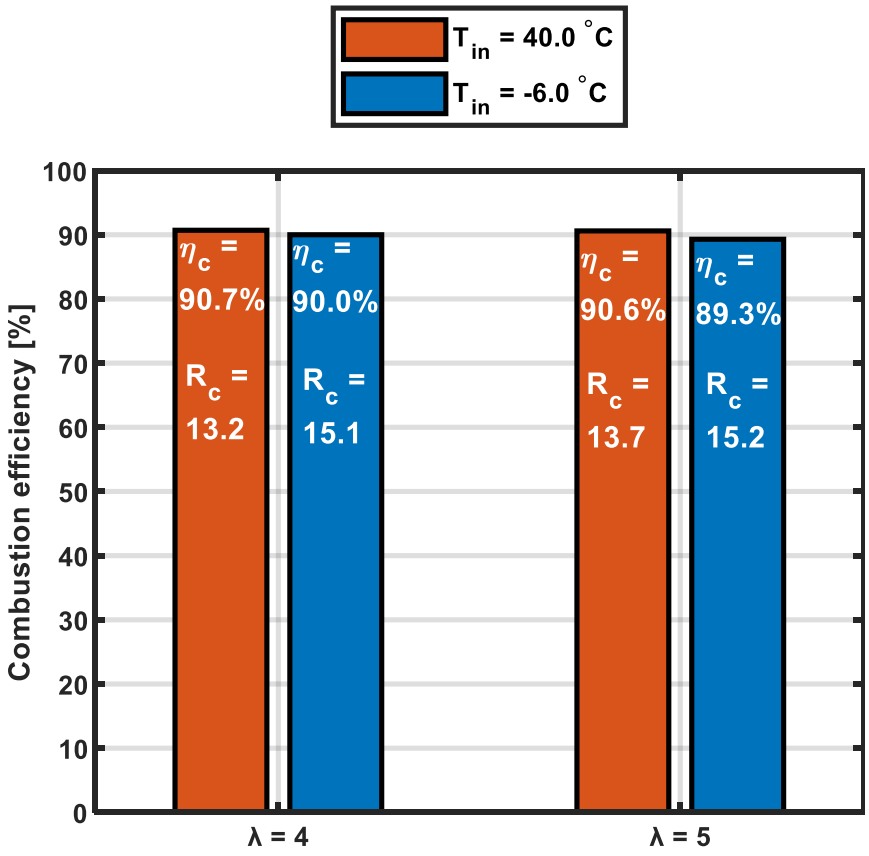

Figure 17: Combustion efficiency for all cases.

The combustion efficiency was calculated as per the following equation:

$$\eta_c = 1 - \frac{\frac{\sum M_i x_i Q_{LHV,i}}{M_p}}{\frac{1}{1+\frac{Ox}{F}} Q_{LHV,f}} \qquad (10)$$

Where:

M_i is the molar mass of species i in the exhaust.

x_i is the mole fraction of species i in the exhaust.

$Q_{LHV,i}$ is the lower heating value of species i in the exhaust.

M_p is the molar mass of products.

$\frac{Ox}{F}$ is the mass oxidizer-fuel ratio (including argon).

$Q_{LHV,f}$ is the lower heating value of fuel.

Mole fractions x_i are obtained from the FTIR analyzer, except for hydrogen molecules which cannot be detected by the FTIR analyzer. Instead, the water gas equation was used to estimate the concentration of hydrogen molecules in the exhaust as follows:

$$x_{H_2} = \frac{x_{CO} x_{H_2O}}{K\, x_{CO_2}} \qquad (11)$$

Where x denotes the concentration of the corresponding molecule and K is the water gas constant that is assumed here to be 3.5 [2]. Cooling the intake and increasing the compression ratio did not, considerably, affect the combustion efficiency.

3.6.2 Gas Exchange Efficiency

Gas exchange efficiency indicates how efficient the process of replacing the burned charge with a fresh one is. Part of the produced energy is lost during this process. The following equation was used to calculate the gas exchange efficiency:

$$\eta_{GE} = \frac{IMEP_n}{IMEP_n + PMEP} \qquad (12)$$

Figure 18 shows the gas exchange efficiency for all cases. It is clear that the gas exchange efficiency slightly decreases as the intake temperature is decreased. This is due to the lower intake pressure of the cooled charge which requires more work for the gas exchange process to take place. Furthermore, as the cases of λ = 5 had slightly lower intake pressure than the cases of λ = 4 (same gaseous flows except for fuel's flow which was lowered to have a leaner mixture), the pumping losses increased and so the gas exchange efficiency decreased.

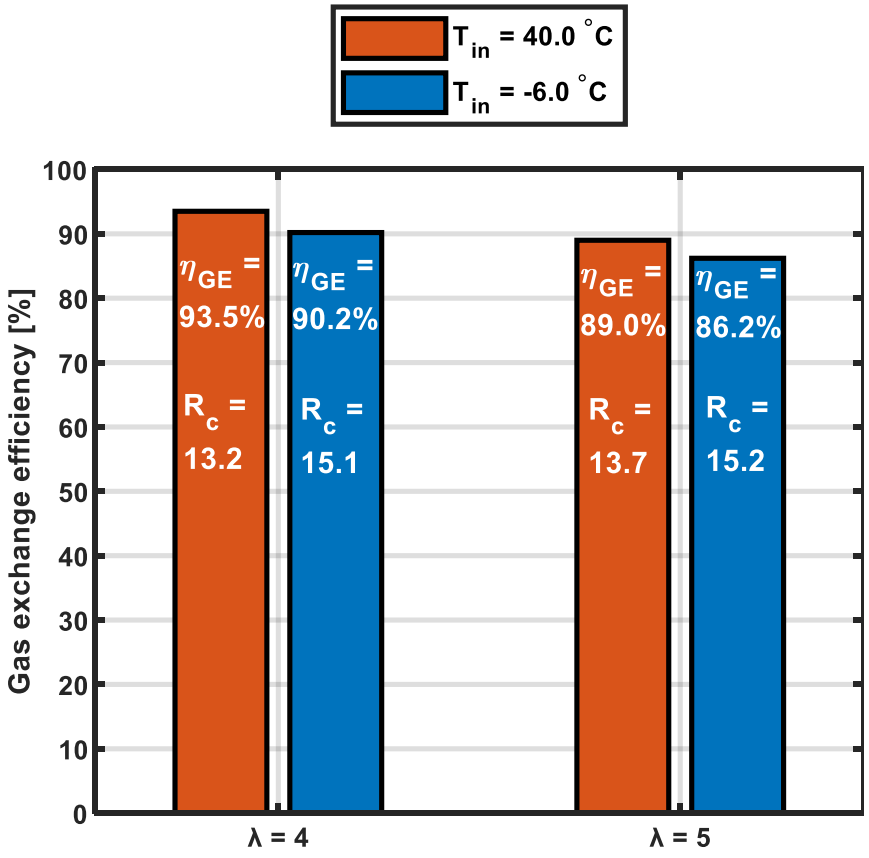

Figure 18: Gas exchange efficiency for all cases.

3.6.3 Thermodynamic Efficiency

Thermodynamic efficiency is the focus of this study. As per Otto's ideal cycle, what is done in this study (increasing the compression ratio and specific heat ratio by using argon) should significantly increase the thermodynamic efficiency as described by the following relation:

$$\eta_{TH,Otto} = 1 - \frac{1}{R_c^{\gamma-1}} \qquad (13)$$

Thermodynamic efficiency can be defined as the ratio of the positive-produced mechanical work on the piston to the amount of heat released in the cylinder, QMEP. The positive-produced mechanical work divided by the displacement volume is sometimes called gross indicated mean effective pressure, IMEPg which is equivalent to the sum of IMEPn and PMEP, i.e., the area enclosed by the P-V diagram corresponding to the positive work only. Thermodynamic efficiency is calculated using the following equations:

$$\eta_{TH} = \frac{IMEP_g}{QMEP} \qquad (14)$$

$$QMEP = \eta_c \cdot FuelMEP \qquad (15)$$

Table 3 summarizes the values of $IMEP_g$ and $QMEP$ for all cases. This will help understand the results of the thermodynamic efficiency shown in Figure 19. The first thing to notice is that $QMEP$ decreased slightly with decreasing the intake temperature

due to the less combustion efficiency. $IMEP_g$ can be expressed as: $QMEP - HTMEP - EXMEP$; referring to Figure 16, it is concluded that HTMEP is the reason why the thermodynamic efficiency decreased in the cooled case of λ = 4. This can be attributed to two reasons; firstly, the increase in compression ratio between the uncooled and cooled cases of λ = 4 (1.9 units) is more than that of the cases of λ = 5 (1.5 units) and as was discussed earlier, higher compression ratios increase the heat transfer losses. The second reason is the increase in the heat transfer coefficient caused by advancing CA50 in the cooled case of λ = 4, as was found in [23]; it was found that at knock regimes in HCCI (like in this study), advancing CA50 by 1 CAD can increase the percentage of the heat transfer losses in the energy distribution by $\sim$ 1.2% due to increasing the heat transfer coefficient. The heat transfer coefficient can increase by roughly 38% by advancing CA50 by only 1.8 CAD. While CA50 in the case of λ = 5 of cooled and uncooled cases is almost the same, the cooled case of λ = 4 has a CA50 that is earlier than that of the uncooled case by $\sim$ 1.2 CAD. Referring to Figure 16, HTMEP, indeed, increased by 2.1% while it did not change for the cases of λ = 5 that had matching combustion phasing.

Table 3: The values of IMEPg and QMEP for all cases

λ	T_{in} [°C]	$IMEP_g$[bar]	QMEP [bar]
4	40.0	2.77	4.87
	-6.0	2.66	4.83
5	40.0	2.03	3.89
	-6.0	2.04	3.83

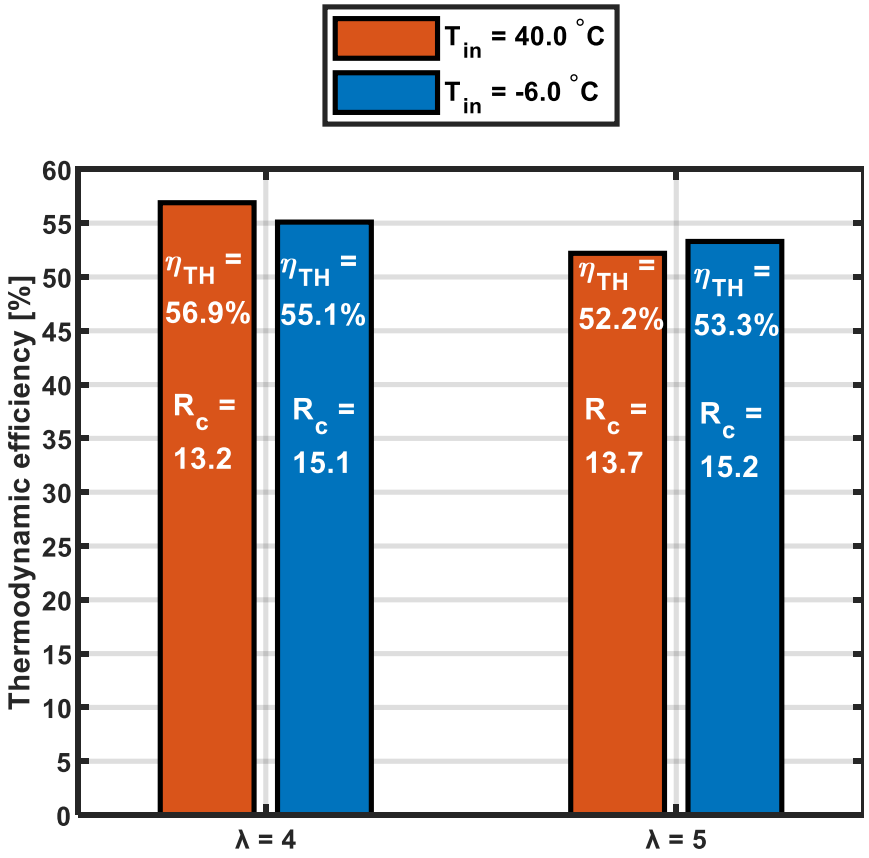

Figure 19: Thermodynamic efficiency for all cases.

Overall, the thermodynamic efficiency is relatively high for all cases due to the use of argon, but it did not change significantly with increasing the compression ratio, and it even deteriorated for the case of λ = 4. This is contrary to what Otto's ideal cycle predicts as described by equation (13). The reason for this disagreement is the assumptions of Otto's cycle that are not applicable in this study such as, isentropic compression and expansion and neglecting heat losses.

3.6.4 Indicated Thermal Efficiency

Indicated thermal efficiency is the efficiency of the engine excluding the mechanical efficiency. It can be calculated as the product of all aforementioned efficiencies as follows:

$$\eta_{Ind} = \eta_c \cdot \eta_{GE} \cdot \eta_{TH} \qquad (16)$$

Figure 20 shows the indicated thermal efficiency of all cases. Since cooling the intake and increasing the compression ratio led to deteriorated combustion, gas exchange, and thermodynamic efficiencies, for all cases (except for the slight increase in thermodynamic efficiency for λ = 5), it is only reasonable for the indicated thermal efficiency to deteriorate as well as it is the product of the three other efficiencies.

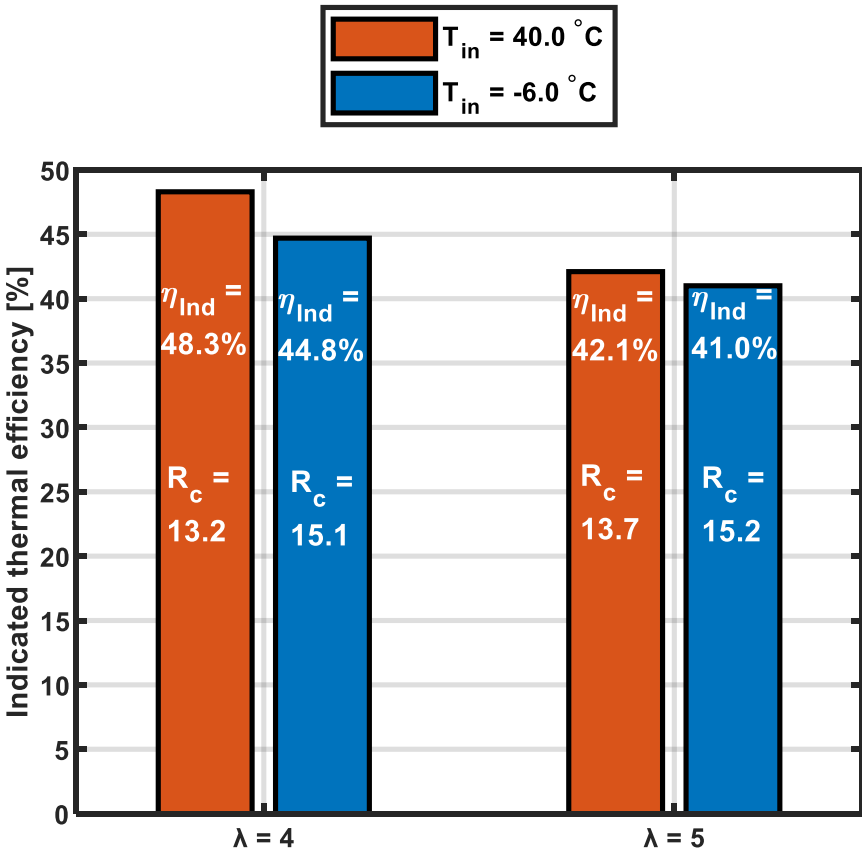

Figure 20: Indicated thermal efficiency for all cases.

Chapter 4: Conclusions

This study examined the potentials of running an argon cycle in HCCI mode at high compression ratios. The main motivation of this experiment is the ideal Otto cycle that predicts achieving high thermodynamic efficiency when the combustion is carried out at high compression ratios and involving reactants with relatively high specific heat ratios. The intake was cooled to counteract the increased in-cylinder temperatures caused by argon which if not counteracted, running at high compression ratios would be damaging to the engine due to advancing the combustion phasing that can cause high pressure rise rates. Two cases were compared, namely, cooled case with high compression ratios, and uncooled case with lower compression ratios. Also, two oxygen/fuel equivalence ratios ($\lambda = 4$ and $\lambda = 5$) were examined in order to investigate more running conditions. The combustion phasing was not of interest here as the maximum compression ratio (knock-limited-compression ratio) was the target of the study. The following conclusions were drawn from the results:

1. The effect of cooling the intake on the combustion phasing (retarding effect) cancelled the effect of increasing the compression ratio (advancing effect). If it was not for this cancelling effect, too high compression ratio would shift the combustion phasing too early (before TDC) which causes negative work on the piston while travelling to the TDC.

2. The developed gamma (specific heat ratio) model showed that cooling the intake charge led to higher specific heat ratio compared to the uncooled charge. Theoretically, this should have a positive impact on the thermodynamic efficiency.
3. The low in-cylinder temperature of the cooled case resulted in less complete combustion than the uncooled case (higher UHC and CO concentrations in the exhaust). This in turn was reflected on the deteriorated combustion efficiency.
4. Having a lower intake pressure, the cooled charge required more work to replace the burned charge with a fresh charge. This was reflected on the deteriorated gas exchange efficiency.
5. Heat losses factor was found to be the main factor affecting the thermodynamic efficiency. Three main factors affected the heat transfer losses, namely, 1) the compression ratio, 2) the in-cylinder temperature, and 3) the heat transfer coefficient and
6. the first and second factors almost cancelled each other as the high compression ratio was accompanied with low in-cylinder temperatures. However, the combustion phasing played an important role in the case of $\lambda = 4$ in affecting the heat transfer coefficient; the cooled case had earlier combustion phasing and hence, higher heat transfer coefficient and more heat losses. This is not applicable for the case of $\lambda = 5$ as the cooled and uncooled cases had almost matching combustion phasing.
7. Overall, the thermodynamic efficiency is relatively high for all cases due to the high specific heat ratio and the high compression ratios. However, increasing the compression ratio brought about a slight improvement in the thermodynamic

efficiency in the case of λ = 5. As for the case of λ = 4, it decreased due to the increased heat losses.

8. As the combustion and the gas exchange efficiencies deteriorated in the cases of high compression ratios (cooled cases) and since the thermodynamic efficiency did not significantly improve (even dropped for λ = 4), the indicated thermal efficiency also deteriorated in the cooled cases.
9. The gas exchange efficiency is the most affected efficiency by cooling. Boosting the intake pressure can considerably improve the indicated thermal efficiency.

BIBLIOGRAPHY

1. Johansson, B., “Förbränningsmotorer,” Eckerle, Lund, 2006.
2. Johansson, B., Andersson, Ö., Tunerstål, P., and Tunér, M., “Combustion Engines,” 1st ed., 2014.
3. Hyvönen, J., Wilhelmsson, C., and Johansson, B., “The Effect of Displacement on Air-Diluted Multi-Cylinder HCCI Engine Performance,” 2006, doi:10.4271/2006-01-0205.
4. Diesel, M., “Two-stroke Low Speed Diesel Engines.”
5. Christensen, M. and Johansson, B., “Influence of Mixture Quality on Homogeneous Charge Compression Ignition,” 1998, doi:10.4271/982454.
6. Christensen, M., Johansson, B., and Einewall, P., “Homogeneous Charge Compression Ignition (HCCI) Using Isooctane, Ethanol and Natural Gas - A Comparison with Spark Ignition Operation,” 1997, doi:10.4271/972874.
7. Christensen, M., Hultqvist, A., and Johansson, B., “Demonstrating the Multi Fuel Capability of a Homogeneous Charge Compression Ignition Engine with Variable Compression Ratio,” 1999, doi:10.4271/1999-01-3679.
8. Onishi, S., Jo, S.H., Shoda, K., Jo, P. Do, and Kato, S., “Active Thermo-Atmosphere Combustion (ATAC) - A New Combustion Process for Internal Combustion Engines,” 1979, doi:10.4271/790501.
9. Anders, H., Christensen, M., Johansson, B., Franke, A., Richter, M., and Aldén, M., “A Study of the Homogeneous Charge Compression Ignition Combustion Process by Chemiluminescence Imaging,” 1999, doi:10.4271/1999-01-3680.
10. Morgan, N.E., Morath, W.D., States., U., and Vickers, I., “Development of a hydrogen-oxygen internal combustion engine space power system,” iv, 200 p., 1965.
11. Underwood, P. and Dieges, P., “Hydrogen and oxygen combustion for pollution free operation of existing standard automotive engines,” *Intersociety Energy Conversion Engineering Conference, p-38, paper*, 1971.
12. Furuhama, S., Yamane, K., and Yamaguchi, I., “Combustion improvement in a hydrogen fueled engine,” *Int. J. Hydrogen Energy* 2(3):329–340, 1977, doi:10.1016/0360-3199(77)90027-1.
13. Laumann, E. and Reynolds, R., “Hydrogen-fueled engine,” 1978.

14. Aznar, M.S., Chorou, F., Chen, J.Y., Dreizler, A., and Dibble, R.W., “Experimental and Numerical Investigation of the Argon Power Cycle,” *Vol. 1 Large Bore Engines; Fuels; Adv. Combust.*, 2019.

15. Sierra Aznar, M., Pineda, D., Cage, B., Corvello, J., Shi, X., Chen, J.-Y., and Dibble, R., “Experimental Investigation of Port and Direct Injection Strategies for Internal Combustion Engines with Argon as the Working Fluid,” 2017, doi:10.17605/OSF.IO/PT67Q.

16. Boer, P.C.T. de and Hulet, J.-F., “Performance of a hydrogen-oxygen-noble gas engine,” *Int. J. HydFfrogen Energy* 5(4):439–452, 1980, doi:10.1016/0360-3199(80)90024-5.

17. Ikegami, M., Miwa, K., and Shioji, M., “A study of hydrogen fuelled compression ignition engines,” *Int. J. Hydrogen Energy* 7(4):341–353, 1982, doi:10.1016/0360-3199(82)90127-6.

18. Mohammed, A.M., Masurier, J.-B., Elkhazraji, A., Dibble, R., and Johansson, B., “A Path towards High Efficiency Using Argon in an HCCI Engine,” 2019, doi:10.4271/2019-01-0951.

19. Woschni, G., “A Universally Applicable Equation for the Instantaneous Heat Transfer Coefficient in the Internal Combustion Engine,” 1967, doi:10.4271/670931.

20. Mcbride, B., Gordon, S., and Reno, M., “Coefficients for Calculating Thermodynamic and Transport Properties of Individual Species,” *Nasa Tech. Memo.* 4513(NASA-TM-4513):98, 1993.

21. Burcat, A. and Ruscic, B., “Third millenium ideal gas and condensed phase thermochemical database for combustion (with update from active thermochemical tables).,” Argonne National Lab.(ANL), Argonne, IL (United States), 2005.

22. Melo, T.C.C. de, Machado, G.B., Belchior, C.R.P., Colaço, M.J., Barros, J.E.M., Oliveira, E.J. de, and Oliveira, D.G. de, “Hydrous ethanol–gasoline blends–Combustion and emission investigations on a Flex-Fuel engine,” *Fuel* 97:796–804, 2012.

23. Dernotte, J., Dec, J.E., and Ji, C., “Energy Distribution Analysis in Boosted HCCI-like / LTGC Engines - Understanding the Trade-Offs to Maximize the Thermal Efficiency,” *SAE Int. J. Engines* 8(3):956–980, 2015, doi:10.4271/2015-01-0824.

24. AVL, Peus Testing

25. Masurier J-B, Elkhazraji A, Mohammed A, Johansson B (2019) HCCI Octane Number Scale in a Pressure-Temperature Diagram. SAE Technical Paper Series. Available: http://dx.doi.org/10.4271/2019-01-0965.

26. Masurier, J.-B., Altoaimi, O., Mohammed, A., Waqas, M. et al., “Combustion Behavior of n-Heptane, Isooctane, Toluene and Blends under HCCI Conditions in the Pressure-Temperature Diagram,” SAE Technical Paper 2018-01-1684, 2018, doi:10.4271/2018-01-1684.

Appendices

Appendix A: Fourier Transform Infrared (FTIR) Analyzer

The infrared radiation is conducted through a sample gas for the non-dispersive IR measurement. Thereby, the molecules contained in the gas absorb a spectrum which is typical for the type of gas. A so-called absorption spectrum is produced. For the IR measurement, the absorbed wavelength range characterises the type of gas while the intensity of the absorption is a measure of the concentration of the measured component as can be seen in Figure 21 [24].

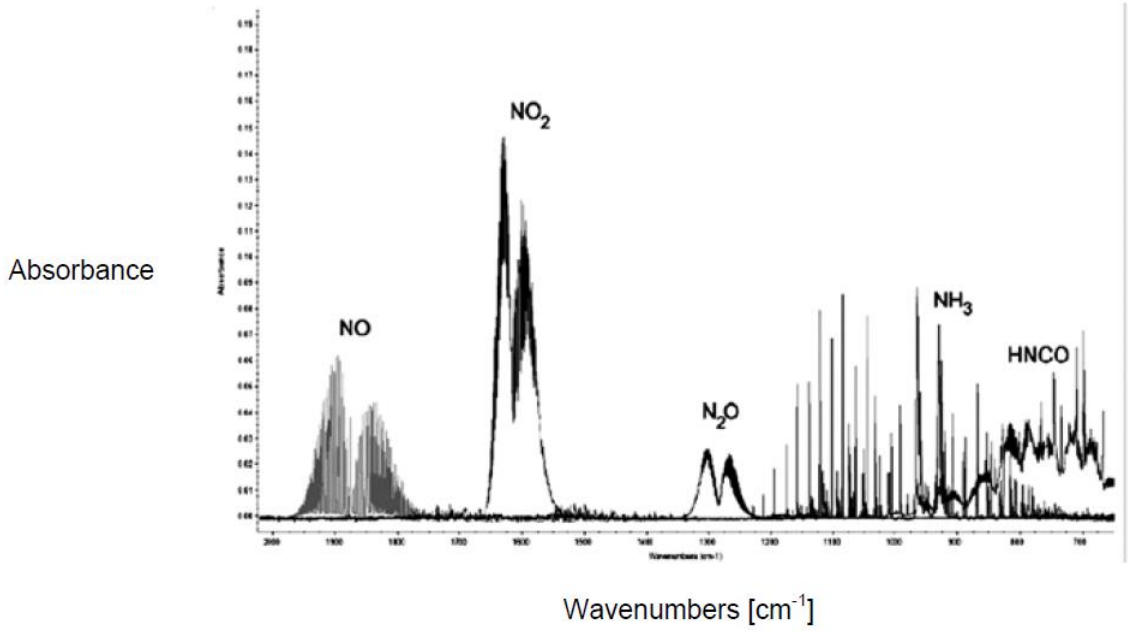

Figure 21: FTIR Infrared Spectrum

The infrared radiation passed through the gas strikes a detector which is filled with the type of gas to be measured. This detector converts the non-absorbed infrared radiation into an electrical signal.

For the concentration determination, it is necessary to conduct the infrared radiation through a comparison gas which does not contain the gas component to be determined, i.e. no absorption occurs at the place of the absorption spectrum to be considered. A "null signal" is determined. The difference between the concentration-dependent measured value and the "null signal" is a measure of the concentration in the sample gas.

Appendix B: Accuracy and Repeatability

Since the experiments involved the use of the relatively expensive gas, that is argon, in high flow rates (79% of the oxygen/argon mixture was argon to mimic the nitrogen percentage in air), it was financially difficult to have multiple runs for each data point. Instead, as a reliability and repeatability check for the provided data extracted from the used CFR engine, this appendix will show results from other experiments (run by the authors of the paper upon which this thesis is based) extracted from the same engine and using the same analysis to show the level of repeatability of the reported data in this thesis. Pressure-temperature (PT) diagrams are the most suitable for this purpose as most of the other results are based on those two variables. The following Figures show the PT diagrams from different experiments, fuels, and conditions. Each data point is repeated three times (total of almost 80 points) and most of them overlap on the PT diagram as can be seen in Figures 22-24 [25, 26]. In these Figures, SOC_L denotes the start of the low temperature combustion, LTC_P denotes the low temperature combustion peak, LTC_M, denotes the inflection point separating the low temperature

and the high temperature combustion, and SOC_M denotes the start of the main combustion.

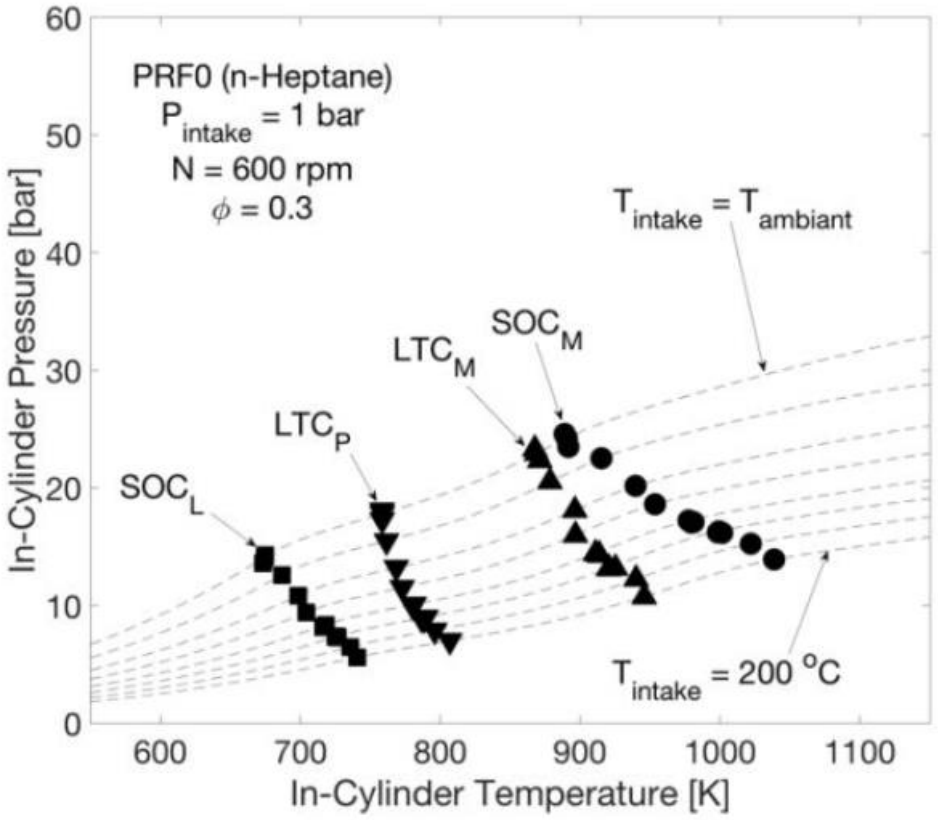

Figure 22: PT diagram for n-heptane at different intake temperatures [25]

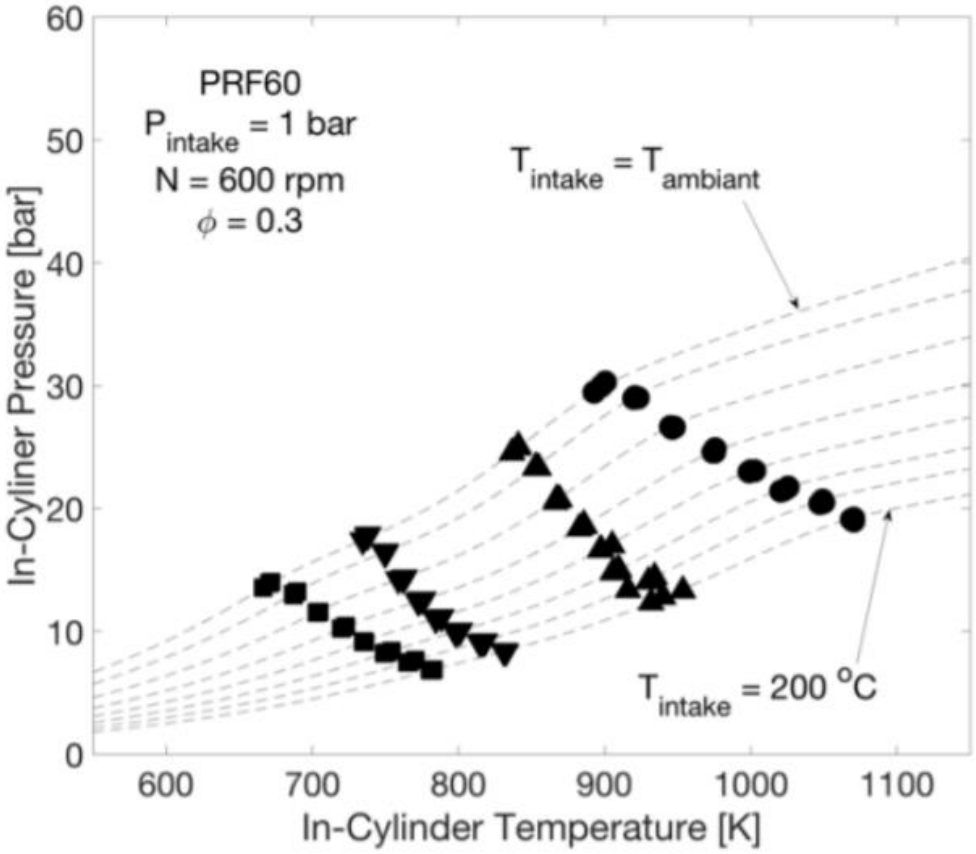

Figure 23: PT diagram for primary reference fuel 60 at different intake temperatures [25]

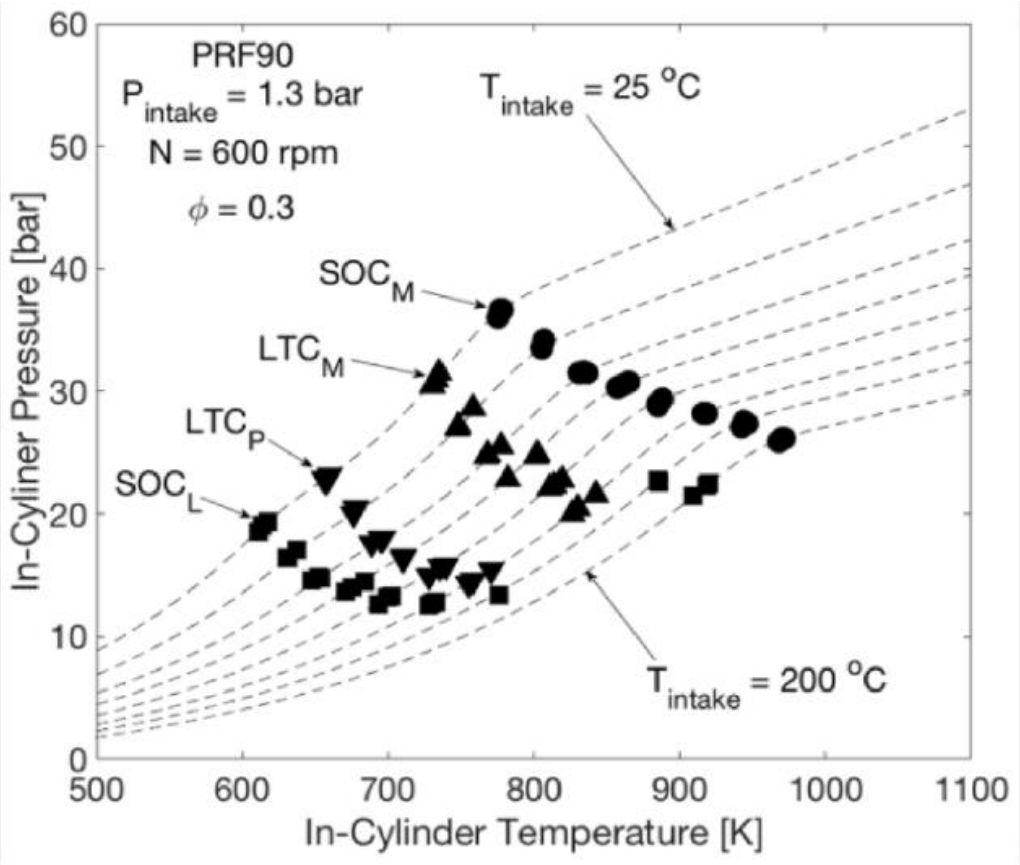

Figure 24: PT diagram for primary reference fuel 90 at different intake temperatures [26]